Soil Dynamics and Earthquake Engineering 41 (2012) 164–180

Contents lists available at SciVerse ScienceDirect

Soil Dynamics and Earthquake Engineering

journal homepage: www.elsevier.com/locate/soildyn

Mechanical behavior of buried steel pipes crossing active strike-slip faults

Polynikis Vazouras [a], Spyros A. Karamanos [b,*], Panos Dakoulas [a]

[a] Department of Civil Engineering, University of Thessaly, Volos 38334, Greece
[b] Department of Mechanical Engineering, University of Thessaly, Volos 38334, Greece

ARTICLE INFO

Article history:
Received 21 February 2012
Received in revised form
14 May 2012
Accepted 15 May 2012
Available online 19 June 2012

ABSTRACT

The present paper addresses the mechanical behavior of buried steel pipes crossing active strike-slip tectonic faults. The pipeline is assumed to cross the vertical fault plane at angles ranging between zero and 45 degrees. The fault moves in the horizontal direction, causing significant plastic deformation in the pipeline. The investigation is based on numerical simulation of the nonlinear response of the soil–pipeline system through finite elements, accounting for large strains and displacements, inelastic material behavior of the pipeline and the surrounding soil, as well as contact and friction on the soil–pipe interface. Steel pipes with D/t ratio and material grade typical for oil and gas pipelines are considered. The analysis is conducted through an incremental application of fault displacement. Appropriate performance criteria of the steel pipeline are defined and monitored throughout the analysis. The effects of various soil and line pipe parameters on the mechanical response of the pipeline are examined. The numerical results determine the fault displacement at which the specified performance criteria are reached, and are presented in diagram form, with respect to the crossing angle. The effects of internal pressure on pipeline performance are also investigated. In an attempt to explain the structural behavior of the pipeline with respect to local buckling, a simplified analytical model is also developed that illustrates the counteracting effects of pipeline bending and axial stretching for different crossing angles. The results from the present study can be used for the development of performance-based design methodologies for buried steel pipelines.

1. Introduction

Permanent ground-induced actions due to earthquakes, such as fault movements, landslides, liquefaction-induced lateral spreading are responsible for the majority of seismic damages in oil and gas buried steel pipelines. Those deformations are applied on the pipeline in a quasi-static manner, and are not necessarily associated with severe seismic shaking, but the pipeline may be seriously deformed in the plastic range, which may lead to pipe wall fracture and loss of containment, with obvious threats to the population and the environment.

The present paper focuses on the structural response of continuous (welded) buried steel pipelines crossing active strike-slip seismic faults. Those pipelines are subjected to an imposed deformation pattern, associated with the development of high stresses and strains in critical locations, which are well beyond the elastic range of pipe material and may cause pipeline failure. In particular, high tensile stresses may cause fracture of the pipeline wall, especially at defected locations or welds, whereas high compression stresses may cause buckling, either in the form of beam-type (global) instability or in the form of pipe wall wrinkling, a shell-type instability, sometimes referred to as "local buckling" or "kinking".

To assess pipeline strength against an imposed strike-slip fault displacement, the state of stress within the pipeline should be calculated for the imposed deformation. Continuing the pioneering paper by Newmark and Hall [1], Kennedy et al. [2,3] developed an analytical model, considering a non-uniform friction interface between the pipe and the soil. Wang and Yeh [4] improved this methodology accounting for pipeline bending stiffness, whereas Vougioukas et al. [5] considered both horizontal and vertical movement of faults and numerically analyzed buried pipes as elastic beams. In later publications, McCaffrey and O'Rourke [6] and Desmod et al. [7] studied the development of strains in buried pipes crossing faults based on the performance of gas and water pipes during the San Fernando earthquake. Wang and Wang [8] studied the problem considering the pipe as a beam on elastic foundation, whereas Takada et al. [9] presented a new simplified method for evaluating the critical strain of the fault crossing steel pipes using the relation between pipe longitudinal deformation with cross-sectional deformation.

The behavior of buried steel pipelines subjected to excessive ground-induced deformations has received significant attention in the pipeline community in the recent years. It has been

* Corresponding author.
E-mail address: skara@uth.gr (S.A. Karamanos).

0267-7261/$ - see front matter © 2012 Elsevier Ltd. All rights reserved.
http://dx.doi.org/10.1016/j.soildyn.2012.05.012

recognized that, apart from the geometric and the mechanical properties of the steel pipeline, site conditions (i.e. the properties of the surrounding soil) may have a strong influence on pipeline response, and that soil–pipe interaction should be taken into account [10]. Kokavessis and Anagnostidis [11], using a finite element methodology and contact elements to describe soil–pipe interaction, analyzed buried pipes under permanent ground-induced actions. Karamitros et al. [12], presented an analytical methodology, refining existing methodologies proposed in [1–4], using a combination of beam-on-elastic-foundation and the beam theory, and computed axial force, bending moment and maximum strain on the pipeline and compared their analytical predictions with results from a three-dimensional finite element model, which employed nonlinear springs to simulate the soil. Liu et al. [13] presented a shell finite element simulation, similar to the model in [12], and reported axial strain predictions along the pipeline. Shitamoto et al. [14] focused on the development of compressive strain limit of X80 pipelines to resist ground-induced actions. They used a solid-element model of a pipe segment, computed the strain corresponding to the maximum moment, and compared this strain capacity to strain demands dictated from soil liquefaction requirements. The seismic analysis of buried and unburied pipelines, under both transient and permanent ground movements have been examined by Arifin et al. [15], using beam finite elements for the pipeline and nonlinear springs to model the effects of the surrounding soil; their analysis resulted in some useful recommendations for mitigating seismic effects. Odina and Tan [16] investigated buried pipeline response under seismic fault displacement, using a beam-type finite element model with elastic–plastic springs for the soil effects. In a subsequent publication, Odina and Conder [17], extended the work in [16] examining the effects of Lüder's plateau of the stress–strain material curve on the pipeline response crossing active faults. A similar methodology for pipelines crossing faults, based on beam-element simulation of the buried pipeline and using nonlinear springs for the surrounding soil, has been presented by Gu and Zhang [18], aiming at determining the optimum crossing angle for the pipeline. More recently, a semi-analytical investigation of buried pipelines behavior under seismic faults has been presented by Trifonov and Cherniy [19], extending the analytical methodology proposed in [12]. The work in [19] has been extended by Trifonov and Cherniy [20] in an attempt to refine the analytical model for inelastic material behavior of the steel pipeline.

In addition to the above numerical studies, notable experimental works on the effects of strike-slip faults on buriedhigh-density polyethylene (HDPE) pipelines have been reported in series of recent papers by Ha et al. [21,22] and Abdoun et al. [23]. This experimental investigation was based on centrifuge modeling of pipeline response to seismic faulting, examining the influence of the type of faulting, the angle of strike-slip faults on the pipeline mechanical behavior, as well as the effects of buried depth and pipeline diameter, and moisture content.

The analytical works outlined above [11–19] have modeled the effects of the surrounding soil through a spring-type approach. A more rigorous approach has been followed by Daiyan et al. [24], who simulated the soil around a non-deformable pipe with elastic–plastic three-dimensional solid finite elements, in an attempt to understand complex soil failure processes and load transfer mechanisms during relative soil–pipeline displacements. In a most recent paper [25], the present authors reported an integrated approach for buried steel pipelines crossing strike-slip faults at right angle with respect to the fault plane, through a finite element modeling of the soil–pipeline system, which accounts rigorously for the inelastic behavior of the surrounding soil, the interaction and the contact between the soil and the pipe (including friction contact and the development of gap), the development of large inelastic strains in the steel pipeline, the distortion of the pipeline cross-section and the possibility of local buckling, the presence of internal pressure. In that work, due to the normality between the pipeline axis and the fault plane, local buckling of pipeline wall was a primary mode of failure, and special emphasis was given in the determination of the corresponding critical fault displacement.

The present paper extends the work presented in [25], considering buried steel pipelines crossing the vertical fault plane at various angles. Furthermore, the paper examines the mechanical behavior of buried steel pipelines with respect to appropriate performance criteria, expressed in terms of local strain or cross sectional deformation. The fault displacement corresponding to each of the performance criteria is identified, in the framework of a performance-based pipeline design. Pipes from two steel grades (X65 and X80), widely used in buried pipeline applications, are considered for typical values of diameter-to-thickness ratio D/t (ranging from 57.6 to 144), in both cohesive and non-cohesive soils. The behavior of internally pressurized pipes with respect to non-pressurized pipes is also examined in terms of each performance criterion. Numerical results are presented in the form of diagrams, depicting the fault displacement corresponding to specific performance criteria with respect to the crossing angle, for typical values of diameter-to-thickness ratio D/t and for specific soil conditions. The present results can be used for developing a performance-based design framework for buried pipelines subjected to permanent ground-induced actions.

2. Performance criteria for buried steel pipelines

The main design requirement of a hydrocarbon pipeline is safety against loss of containment. Under strong permanent ground-induced actions, buried steel pipelines exhibit severe deformation beyond the elastic limit. Steel material is ductile and capable of sustaining significant amount of inelastic deformation, but at locations where large tensile strains develop, rupture of the pipeline wall may occur. Wrinkling (local buckling) of pipeline wall may also occur due to excessive compression at the pipeline wall, followed by pipe wall folding and development of significant local strains. Furthermore, severe distortions of the pipeline cross-section may render the pipeline non-operational.

To quantify the amount of damage in a buried pipeline under severe ground-induced action, appropriate performance criteria (quite often referred to as "limit states"), should be adopted. One should note that the pipeline design has been traditionally based on the "allowable stress" concept. However, in the case of extreme ground-induced loading conditions, which act on the pipeline under deformation-controlled conditions, the pipeline exhibits significant inelastic deformation. Therefore, pipeline performance should be addressed in terms of limit states based on strain or deformation, rather than stress. Based on the above discussion, the following performance limit states are described and quantified below: (a) tensile strain in the longitudinal direction of the pipeline that causes pipe wall rupture, (b) local buckling (wrinkling) formation, and (c) excessive distortion of the pipeline cross-section.

2.1. Maximum tensile strain

Determination of tensile strain capacity of a pipeline is of primary importance for establishing an efficient strain-based pipeline design procedure. In the absence of serious defects and damage of the pipeline, the tensile capacity is controlled mainly by the strength of the girth welds, which are usually the weakest

locations due to weld defects and stress/strain concentrations. Tensile strain limits are experimentally determined through appropriate tension tests on strip specimens and in wide plates [26]. For design purposes, a simple and straightforward approach for determining tensile strain limit of girth welds in pipeline is provided by CSA Z662 pipeline design standard, Annex C [27], through the following equation that considers surface-breaking defects:

$$\varepsilon_{Tu} = \delta^{(2.36-1.583\lambda-0.101\xi\,\eta)}(1+16.1\lambda^{-4.45})(-0.157+0.239\xi^{-0.241}\eta^{-0.315}) \quad (1)$$

where, ε_{Tu} is the ultimate tensile strain capacity in %, δ is the CTOD toughness of the weld ($0.1 \le \delta \le 1$), λ is the yield-to-tensile strength ratio ($0.7 \le \lambda \le 0.95$), ξ is the ratio of defect length over the pipe wall thickness ($2c/t$) with $1 \le \xi \le 10$, and η is the ratio of defect height over the pipe wall thickness (a/t) with $\eta \le 0.5$. Background information for Eq. (1) can be found in the paper by Wang et al. [28]. Considering a slightly defected pipe, with $\xi=1.0$, $\eta=0.1$, $\delta=0.7$ and $\lambda=0.775$, one obtains a value of $\varepsilon_{Tu}=4.5\%$. In the following, two values for the ultimate tensile strain ε_{Tu} are considered, namely 3% and 5%. It is noted that the first value is also adopted by the EN 1998-4 provisions for seismic-fault-induced action on buried steel pipelines [40] and by the seismic provisions of ASCE MOP 119 for buried water steel pipelines [41].

2.2. Local buckling

Under ground-induced actions, together with the development of tensile strains on the pipeline wall, compressive strains (due to pipe bending deformation) may also occur. When compressive strains exceed a certain limit, pipeline wall exhibits structural instability in the form of local buckling or wrinkling. In the presence of those "wrinkles" or "buckles", the pipeline may still fulfill its transportation function, provided that the steel material is adequately ductile [41]. However, the buckled area is associated with significant strain concentrations and, in the case of repeated loading (e.g. due to variations of internal pressure or temperature), fatigue cracks may develop, imposing a serious threat for the structural integrity of the pipeline [42,43]. Therefore, the formation of a local buckle or wrinkle can be considered as a limit state. Extensive research on axial compression and bending of steel pipe segments has demonstrated that compressive strain limits for steel pipes depend on the diameter-to-thickness ratio (D/t), the yield stress of steel material σ_y, the presence of internal or external pressure, as well as the initial imperfections and the residual stresses (as a result of the manufacturing process). A brief overview of this research is presented in the recent paper of Gresnigt and Karamanos [30]. The local buckling strain ε_{Cu} can be estimated using the following design equation:

$$\varepsilon_{Cu} = 0.5\left(\frac{t}{D}\right) - 0.0025 + 3000\left(\frac{\sigma_h}{E}\right)^2 \quad (2)$$

where the hoop stress σ_h depends on the level of internal pressure p:

$$\sigma_h = \begin{cases} \dfrac{pD}{2t}, & \text{if } \dfrac{pD}{2t\sigma_y} \le 0.4 \\ 0.4\sigma_y, & \text{if } \dfrac{pD}{2t\sigma_y} > 0.4 \end{cases} \quad (3)$$

Eq. (2) has been initially proposed in [29], and has been adopted by the recent CSA Z662 specification [27].

2.3. Distortion of pipeline cross-section

In order to maintain the pipeline operational, it is necessary to avoid significant distortions of the pipeline cross-section. A simple and efficient measure of cross-sectional distortion is ovalization, quantified through the so-called non-dimensional "flattening parameter" f defined as follows:

$$f = \frac{\Delta D}{D} \quad (4)$$

Following the suggestion in [29], a cross-sectional flattening limit state is reached when the value of the above parameter f becomes equal to 0.15, a value also adopted by the Dutch specification NEN 3650 [31].

3. Numerical modeling

The structural response of steel pipelines under strike-slip fault movement is examined numerically, using the general-purpose finite element program ABAQUS [32]. The nonlinear material behavior of the steel pipe and the surrounding soil, the interaction between the soil and the pipe, as well as the distortion of the pipeline cross-section and the significant deformation of the surrounding soil are modeled in a rigorous manner, so that the pipeline performance criteria are evaluated with a high-level of accuracy.

The finite element model is an enhancement of the model presented in [25]. The pipeline is embedded in an elongated soil prism along the x axis shown in Fig. 1a. Fig. 1b shows the soil mesh in the y–z plane and Fig. 1c depicts the mesh for the steel pipe. Four-node reduced-integration shell elements (type S4R) are employed for modeling the cylindrical pipeline segment, and eight-node reduced-integration "brick" elements (C3D8R) are used to simulate the surrounding soil. The top surface of the prism represents the soil surface, and the burial depth is chosen equal to about 2 pipe diameters, which is in accordance with pipeline engineering practice [33]. The prism length in the x direction is equal to at least 65 pipe diameters, whereas dimensions in directions y, z equal to 11 and 5 times the pipe diameter respectively. These dimensions are in accordance with the model dimensions in [25].

The central part of the pipeline, where maximum stresses and strains are expected, has a fine mesh of shell elements. In accordance with the analysis in [25], a total of 54 shell elements around the cylinder circumference in this central part have been found to be adequate to achieve convergence of solution, whereas the size of the shell elements in the longitudinal direction has been chosen equal to 1/26 of the pipeline outer diameter D. This mesh has been shown capable of describing the formation of short-wave wrinkling (local buckling) on the pipeline wall. The mesh chosen for the pipe parts far from the fault location is significantly coarser. Similarly, the finite element mesh for the soil is more refined in the region near the fault and coarser elsewhere.

The seismic fault plane divides the soil in two blocks of equal size (Fig. 1a). The analysis is conducted in two steps as follows; gravity loading is applied first and subsequently, fault movement is imposed, using a displacement-controlled scheme, which increases gradually the fault displacement d. The nodes on the vertical boundary planes of the first block (pipe and soil nodes) remain fixed in the horizontal directions. A uniform horizontal displacement due to fault movement is imposed at the external nodes (pipe and soil) of the second (moving) block along the horizontal n direction, which is parallel to the fault plane, whereas the motion along the vertical direction is not restrained. In addition, at both blocks all nodes on the bottom boundary

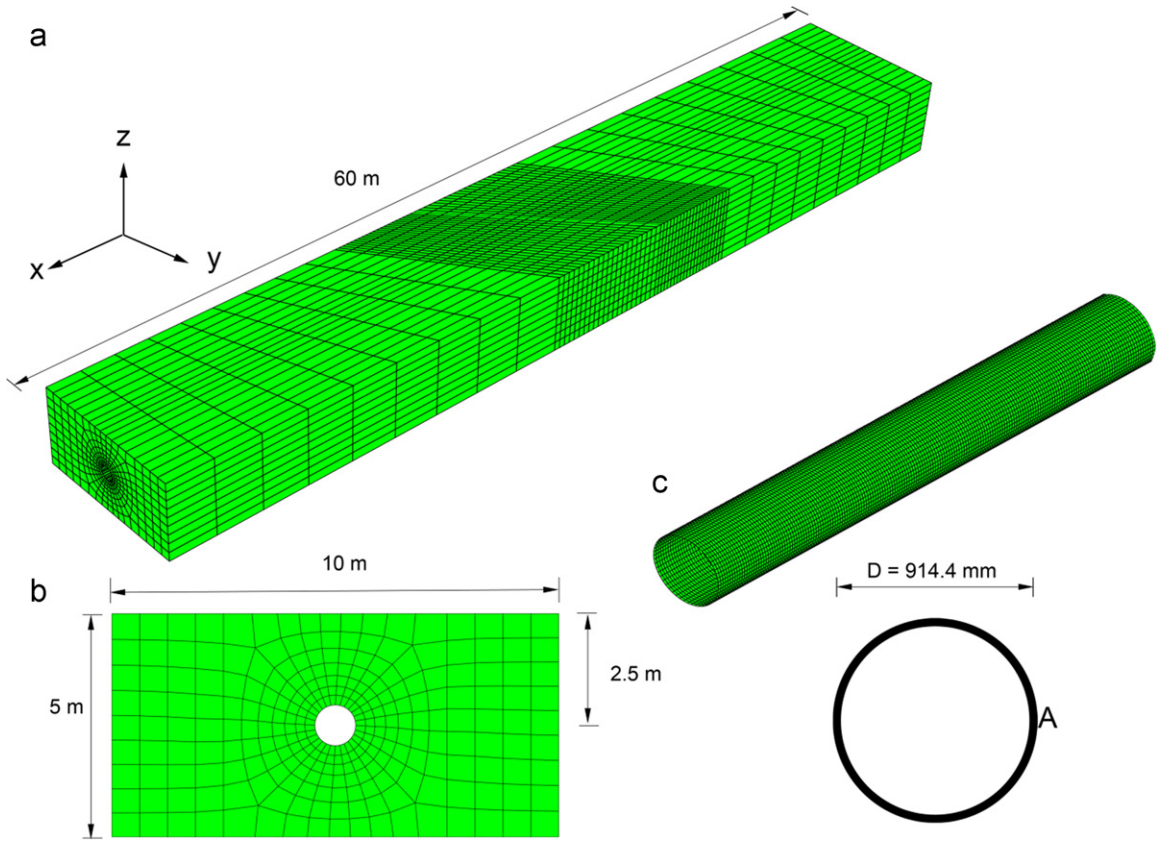

Fig. 1. Finite element model of the (a) soil prism with tectonic strike-slip fault, (b) finite element mesh of soil prism cross-section and (c) finite element mesh of steel pipeline.

plane are fixed with respect to vertical displacement to eliminate rigid body motion. For the case of pressurized pipelines an intermediate step of internal pressure application is considered (after the application of gravity and before the fault displacement is activated).

Fig. 2a plots the soil–pipeline system after a seismic fault movement in the horizontal direction. The angle β between the fault direction n and the direction y (shown in Fig. 3) is a key parameter of the present numerical study. Positive values of β indicate that the fault movement induces tension to the pipeline, whereas negative values of β refer to fault movements that result in pipeline compression. To overcome numerical complications due to discontinuity at the vicinity of the fault, the fault movement is considered to occur within a narrow transverse zone of width w, a common practice in several recent numerical studies of fault-foundation interaction [34–36], also corresponding to a more realistic representation of the fault displacement mechanism [37]. A relevant numerical investigation in [25] has shown that a value of w equal to 0.33 m is adequate for the purposes of the present analysis.

A large-strain von Mises plasticity model with isotropic hardening is employed for the steel pipe material, and its calibration is performed through an appropriate uniaxial stress–strain curve from a tensile test on a coupon specimen from the pipeline material. Furthermore, the mechanical behavior of soil material is described through an elastic-perfectly plastic Mohr–Coulomb constitutive model, characterized by the cohesion c, the friction angle ϕ, the elastic modulus E, and Poisson's ratio ν. The dilation angle ψ is assumed equal to zero for all cases considered in this paper.

The interface between the outer surface of the steel pipe and the surrounding soil is simulated with a contact algorithm, which allows separation of the pipe and the surrounding soil, and accounts for interface friction, through an appropriate friction coefficient μ. In the majority of results reported in the present study, the value of μ is considered equal to 0.3, a value also adopted in [25]. A short sensitivity of the results on the value of μ is offered in the next section.

During the consecutive stages of fault displacement, the performance criteria are evaluated, monitoring the maximum values of longitudinal and hoop strain along the pipeline, as well as the cross-sectional distortion (flattening) at critical locations. Furthermore, the finite element model is capable of simulating rigorously the formation of pipeline wall wrinkling.

4. Numerical results

Numerical results are obtained for X65 and X80 steel pipelines for typical values of the diameter-to-thickness ratio, and for different soil conditions. The outer diameter D of the pipe is equal to 914.4 mm (36 in.), which is a typical size for oil and gas transmission pipelines. Four values for the pipe wall thickness are considered, namely 6.35 mm ((1/4) in.) 9.53 mm ((3/8) in.), 12.7 mm ((1/2) in.) and 15.88 mm ((5/8) in.), corresponding to D/t values equal to 144, 96, 72 and 57.6 respectively, which cover a wide range of oil and gas pipeline applications. Note that the first value corresponds to relatively thin-walled pipes ($D/t=144$), which may also be used for water transmission pipelines.

The soil–pipeline model has dimensions 60 m × 10 m × 5 m in directions x, y, z respectively, which complies with the size requirements stated in the previous section. The seismic fault plane passes through the middle cross-section of the pipeline and crosses the pipeline axis at different angles, so that the value of angle β ranges between -10 degrees and 45 degrees, as shown in

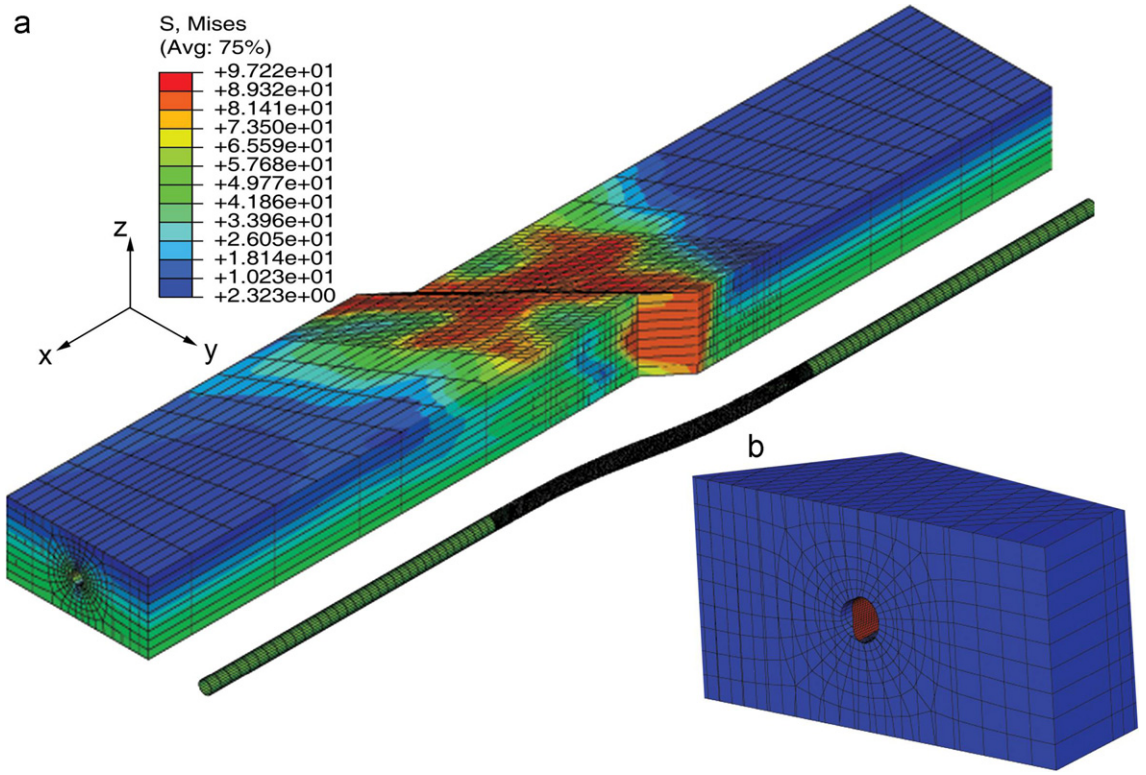

Fig. 2. (a) Deformation of the pipeline–soil system after application of fault displacement; finite element results depict the von Mises stress. (b) Detailed view of fault displacement with detachment of pipeline from the soil.

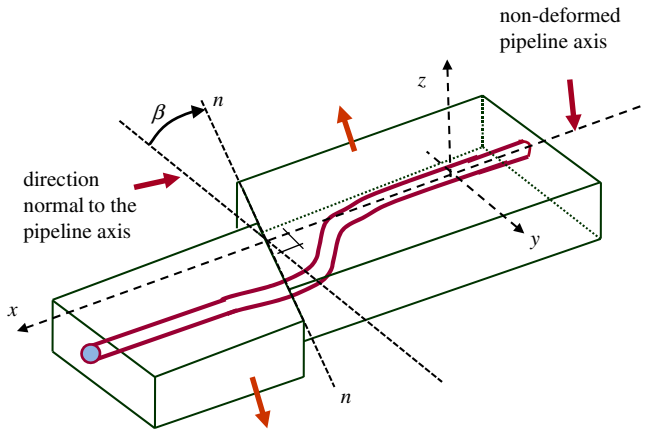

Fig. 3. Schematic representation of a pipeline crossing a strike slip fault at a crossing angle β.

Fig. 3, where the minus sign indicates a configuration where the pipeline is subjected to global compression.

In Sections 4.1 and 4.2, non-pressurized X65 pipelines are analyzed under cohesive and non-cohesive soil conditions respectively, whereas in Section 4.3 the effects of internal pressure are investigated. Finally, in Section 4.4, the structural response of high-strength X80 steel pipelines is examined, including the effects of internal pressure.

4.1. Non-pressurized X65 steel pipelines in cohesive soils

Buried X65 steel 36-in.-diameter pipelines are examined first, in the absence of internal pressure, considering cohesive soil conditions, with appropriate values of soil parameters c, φ and E. The API 5L X65 steel material is a typical steel material for oil and

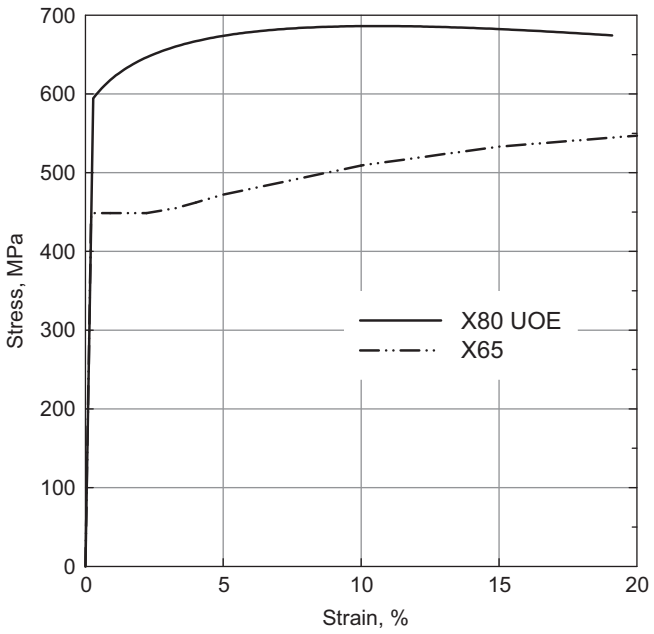

Fig. 4. Uniaxial nominal stress-engineering strain curve for X65 and X80 linepipe steel.

gas pipeline applications, with a nominal stress-engineering strain curve shown with dashed line in Fig. 4, obtained from a uniaxial tensile test. The yield stress σ_y is equal to 448.5 MPa (65 ksi) followed by a plastic plateau up to 1.48% strain and, subsequently, by a strain-hardening regime with a hardening modulus equal to about $E_s/300$, where E_s is the Young's modulus of the steel material, equal to 210 GPa. Considering a safety (reduction) factor equal to 0.72, as suggested in [38,39], the

maximum operating pressure p_{max} of this pipeline, given by the following expression:

$$p_{max} = 0.72 \times \left(2\sigma_y \frac{t}{D}\right) \quad (5)$$

is plotted in terms of the D/t value with the dashed line in Fig. 5.

A buried steel pipeline with wall thickness equal to (3/8)-in., embedded in a soft-to-firm clay soil is considered first. This clay is referred to as Clay I and, under "undrained" loading conditions, it has a cohesion $c=50$ kPa, friction angle $\varphi=0^{\circ}$, Young's modulus $E=25$ MPa and Poisson's ratio $v=0.5$. Fig. 6(a) depicts the shape of the deformed pipeline at fault displacements $d=0.4$ m, 1.37 m, 2 m and 2.9 m in the area near the fault, crossing the fault at a right angle, i.e. the β angle is equal to zero degrees. Moreover, Fig. 6(b) depicts the shape of the deformed pipeline and the distribution of the longitudinal normal strain ε_x on its outer surface at the same four values of fault displacement. At a value of fault displacement equal to $d=0.43$ m, the pipeline wall exhibits local buckling, in the form of a short-wave wrinkling pattern. It should be noted that the wrinkling pattern is formed gradually with increasing fault displacement, so that a criterion is necessary for identifying the deformation stage at which the onset of local buckling occurs. In the present study, the onset of buckling is defined as the stage where outward displacement of the pipe wall starts at the area of maximum compression, a criterion also adopted in [25], and the corresponding fault displacement is referred to as "critical fault displacement" (d_{cr}).

At that stage, bending strains due to pipe wall wrinkling develop, associated with significant tensile strains at the "ridge" or "crest" of the buckle, so that the longitudinal compressive strains at this location at the outer surface of the pipe wall start decreasing, forming a short wavy pattern at this location. At the onset of local buckling, the longitudinal compressive strain at the buckle location (ε_{cr}) is equal to 6.90×10^{-3}, which is considerably higher than the corresponding value of 2.71×10^{-3} predicted by Eq. (2). Furthermore, the maximum tensile strain on the opposite side of the pipe ($\varepsilon_{T,max}$) is 3.54×10^{-3}, which is substantially lower than the strain that would cause tensile failure in the form of rupture in a non-seriously-defected pipeline.

Under increasing fault displacement the wrinkled pattern develops further, resulting in a significant localization of deformation at the buckled area. However, this wrinkle development occurs up to a fault displacement equal to 1.37 m, whereas beyond this value, the depth of the buckle (i.e. the wrinkling wave amplitude) starts decreasing due to longitudinal stretching of the pipeline, as shown in Fig. 6(b) for values of fault displacements d equal to 1.37 m and 2.9 m. Furthermore, as the total pipeline length increases with continued fault movement due to longitudinal stretching, it results to higher tensile strains in the longitudinal direction, whereas the corresponding compressive strains become smaller. This is shown in Fig. 6(b), where for a fault displacement of $d=2.9$ m, compressive longitudinal strains are significantly lower than those corresponding to a fault displacement of $d=1.4$ m. The overtaking of the tensile strains after some critical value of d has also been identified in [25], and is illustrated through a simplified model in Section 5. The variations of longitudinal compressive and tensile strain ε_x along the two outer (most stressed) generators of the pipe cylinder are shown in Figs. 7 and 8 for a small segment of the pipeline about the critical area and for different values of the fault displacement.

Beyond the formation of the local buckle, and for fault displacement greater than 1.50 m, significant distortion of the cross-section in terms of ovalization is observed. The pipeline cross-section with maximum distortion is located at a distance of 0.5 m from the fault, and the corresponding flattening parameter reaches the critical value of 0.15 at a fault displacement equal to $d=1.71$ m. In addition, the maximum tensile longitudinal strain of the pipe is significantly increased, on either side of the pipeline cross-section, which may lead to local fracture at welds or at locations of minor defects. For a fault displacement of $d=1.62$ m, the maximum tensile strain is equal to 3%, a critical value as discussed above. At the end of the analysis (fault displacement equal to 4 m), the longitudinal tensile strain limit of 5% has not been reached at any location of the pipeline wall.

The above results have been obtained with a value of friction coefficient μ equal to 0.3. A small sensitivity study of the results has also been conducted for values of μ between 0.15 and 0.45. The corresponding value of the critical displacement d_{cr} varies from 0.46 m (for $\mu=0.15$) to 0.42 m (for $\mu=0.45$), a rather small effect. In the following, the value of friction coefficient μ is assumed equal to 0.3.

The 36-in.-diameter (3/8)-in.-thick X65-steel pipeline, embedded in the same soft-to-firm clay soil conditions (Clay I), is also examined for various crossing angles. Fig. 9 shows the deformed

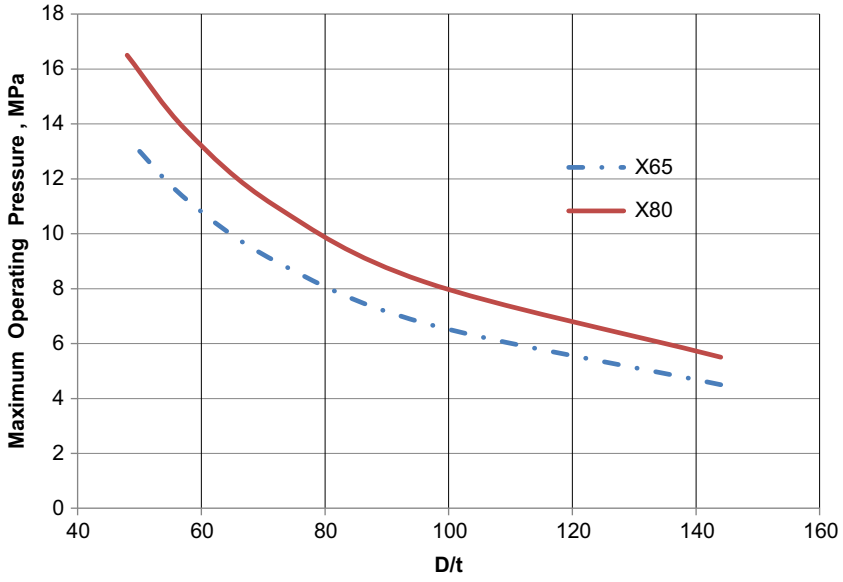

Fig. 5. Variation of maximum operating pipeline pressure with respect to the diameter-to-thickness ratio D/t.

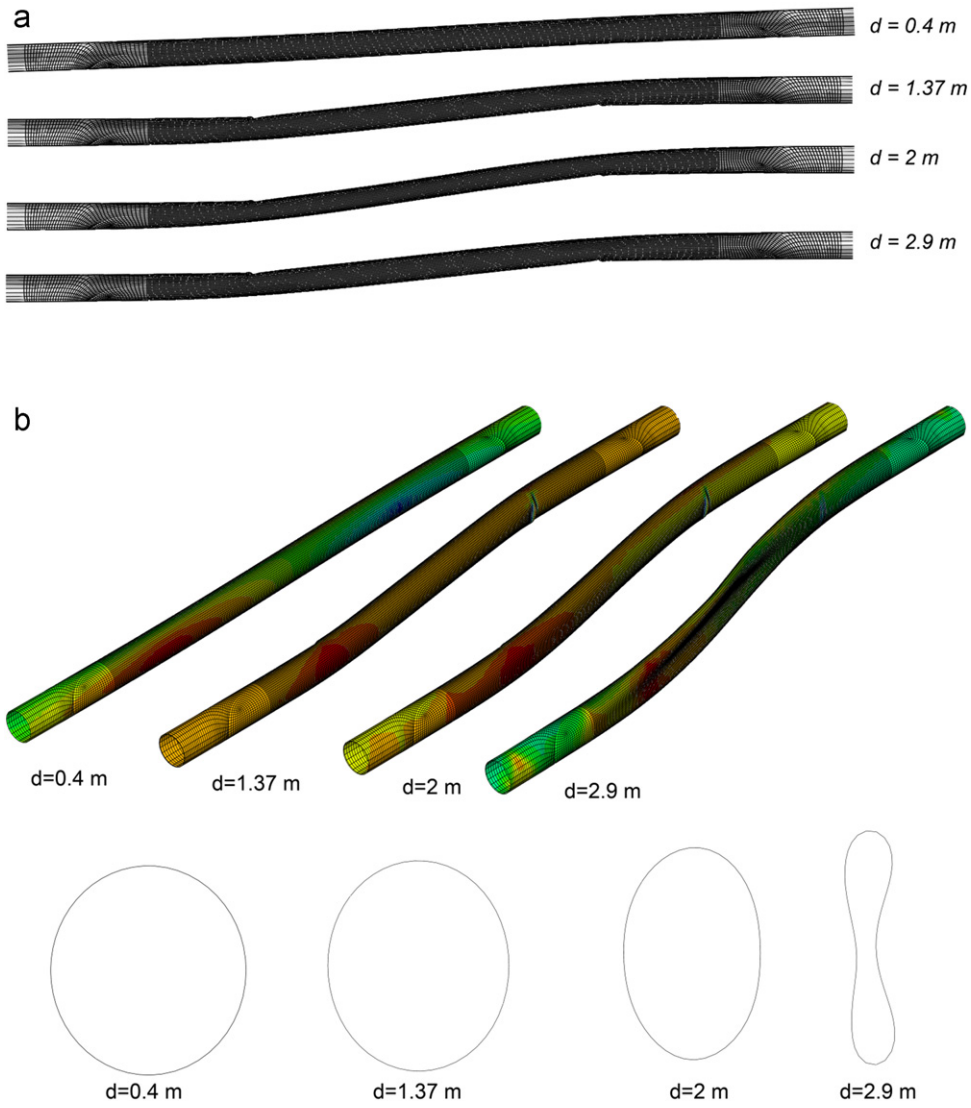

Fig. 6. (a) Plan view of deformed shapes for an X65 $D/t=96$ pipeline in Clay I conditions and $\beta=0$, for various values of fault displacement; (b) distribution of longitudinal strain and (c) corresponding cross-sectional deformation at 0.5 m from the fault.

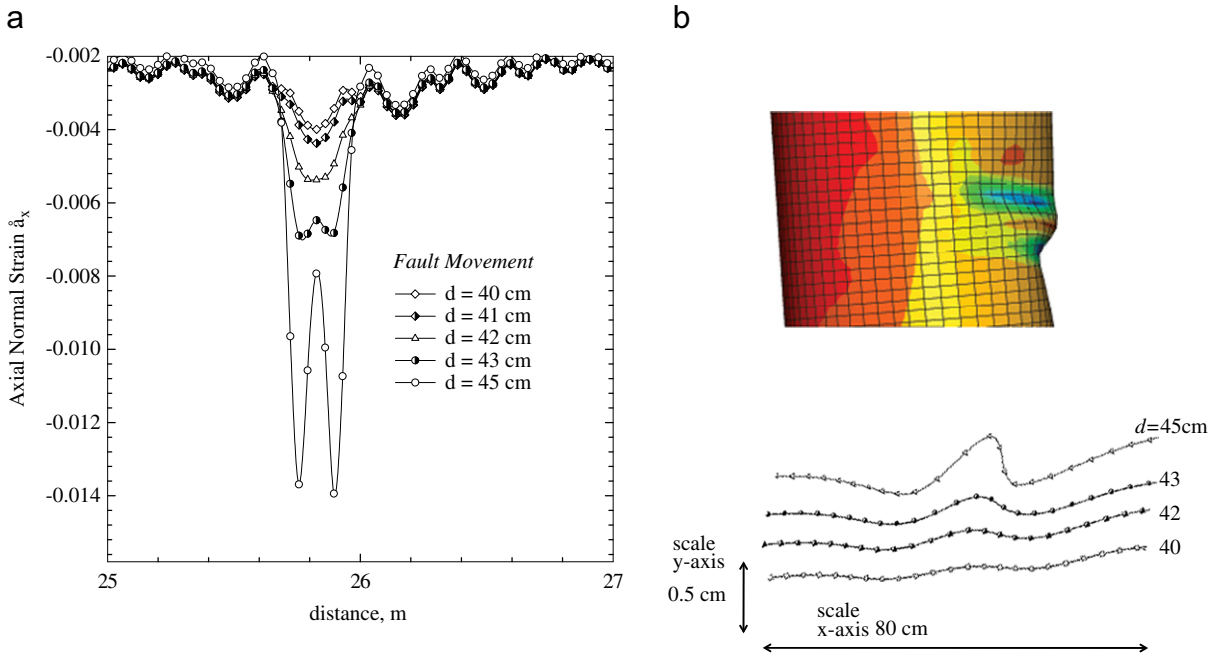

Fig. 7. (a) Variation of axial strain and critical pipeline generator at the compression side of the buckled area for different values of fault displacement and (b) evolution of wall wrinkling (X65 $D/t=96$ pipeline in Clay I conditions and $\beta=0$).

shapes of the pipeline for a value of β equal to 25 degrees, at various fault displacements. At this angle, local buckling of the pipeline wall does not occur. The deformed shape shows a significant distortion of the pipeline cross-section in the form of ovalization. The amount of ovalization, measured according to the flattening parameter f, reaches a critical value of 0.15 at fault displacement of 0.77 m, at the area where the pipe intersects with the fault. Under increasing fault movement, this ovalization pattern is further developed resulting in a severe distortion of the pipe cross-section (Fig. 9), associated with negative hoop curvature of the pipeline wall, sometimes referred to as "inversion", for a fault displacement of $d=1.45$ m. The critical longitudinal tensile strain limits of 3% and 5% appear at a fault displacements $d=0.58$ m and 1.15 m respectively, one meter away from fault.

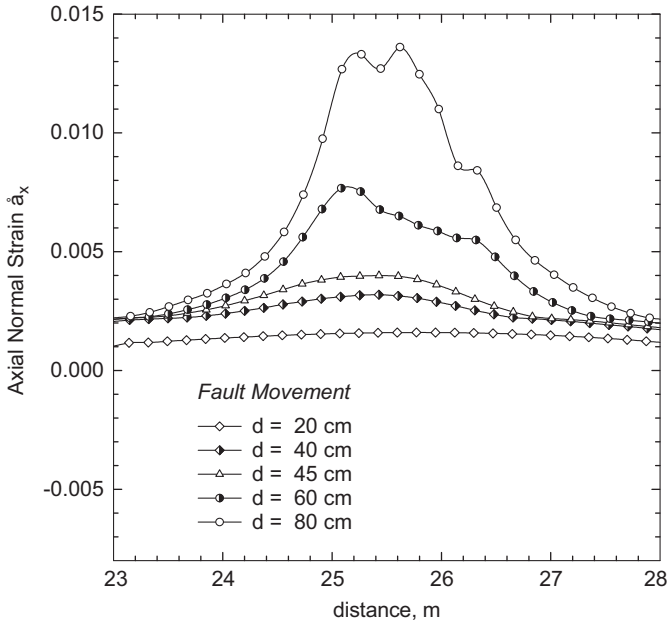

Fig. 8. Variation of axial strain at the tension side of the buckled area for different values of fault displacement (X65 $D/t=96$ pipeline in Clay I conditions and $\beta=0$).

The above X65 (3/8)-in.-thick steel pipeline in Clay I soil conditions, is also analyzed for the case of crossing the fault plane at an angle of β equal to 45 degrees. The deformed shapes of the pipeline are shown in Fig. 10 for fault displacement values equal to 0.5 m, 1 m, 1.5 m, 2 m. Maximum longitudinal tensile strain occurs at the cross-section where the pipeline crosses the fault plane and reaches the critical values of 3% and 5% at fault displacements $d=0.335$ m and 0.885 m, respectively. Furthermore, the cross-sectional flattening parameter f reaches the critical value of 0.15 at fault displacement of 0.74 m, at the area where the pipeline intersects the fault plane. Under increasing fault movement, this flattening pattern develops further as shown in Fig. 10, resulting into an inversion of the pipeline wall, for a fault displacement of $d=1.80$ m.

The response of the pipeline becomes quite different if a crossing angle β of negative sign is considered. In this case, the fault motion is associated with a decrease of length of the pipeline, resulting in the development of significant compressive stresses and strains, leading to local buckling. In Fig. 11, the performance of the above (3/8)-in.-thick X65-steel pipeline is shown for Clay I soil conditions, crossing the fault plane at an angle of β equal to -10 degrees. The critical fault displacement at which wrinkling initiates has been computed equal to 0.225 m at a distance of 3.6 m away from fault. At this point the values of compressive strain at buckle is -5.32×10^{-3}, higher than the value of -2.71×10^{-3} predicted by Eq. (2), whereas the corresponding maximum tensile strain on the opposite side of the pipeline wall is equal to 1.01×10^{-3}. Upon continuation of fault displacement, the buckle pattern is further developed resulting in folding of the pipeline wall and inversion of the buckled cross-section at fault displacement $d=0.75$ m. Tensile strain of 3% occurs at fault displacement $d=0.49$ m and 5% at $d=0.67$ m, and the ovalization performance criterion is reached at $d=2.3$ m, at a distance of 0.5 m from the fault.

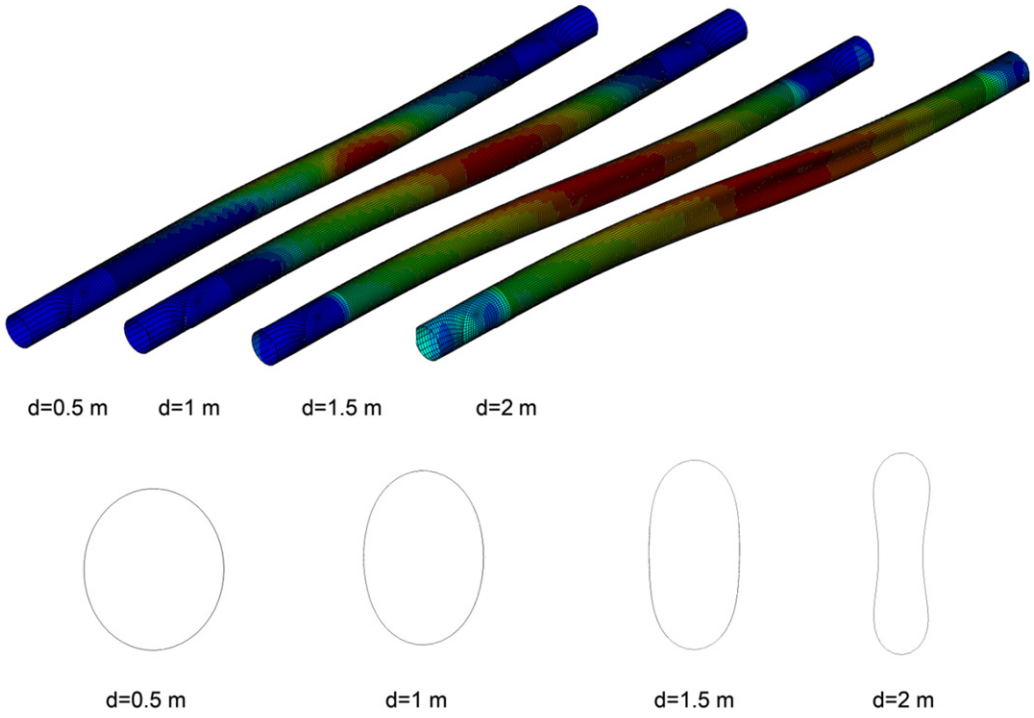

Fig. 9. (a) Deformed shapes and distribution of longitudinal strain for an X65 $D/t=96$ pipeline in Clay I conditions and $\beta=25^\circ$, for various values of fault displacement and (b) corresponding cross-sectional deformation at 0.5 m from the fault.

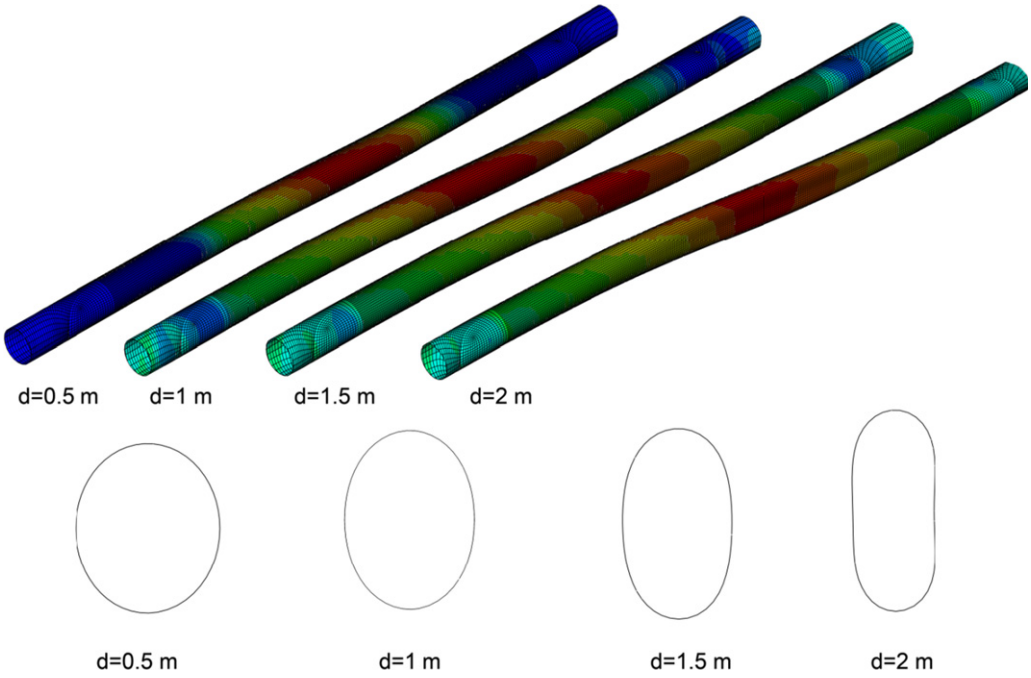

Fig. 10. (a) Deformed shapes and distribution of longitudinal strain for an X65 $D/t=96$ pipeline in Clay I conditions and $\beta=45^{\circ}$, for various values of fault displacement and (b) corresponding cross-sectional deformation at 0.5 m from the fault.

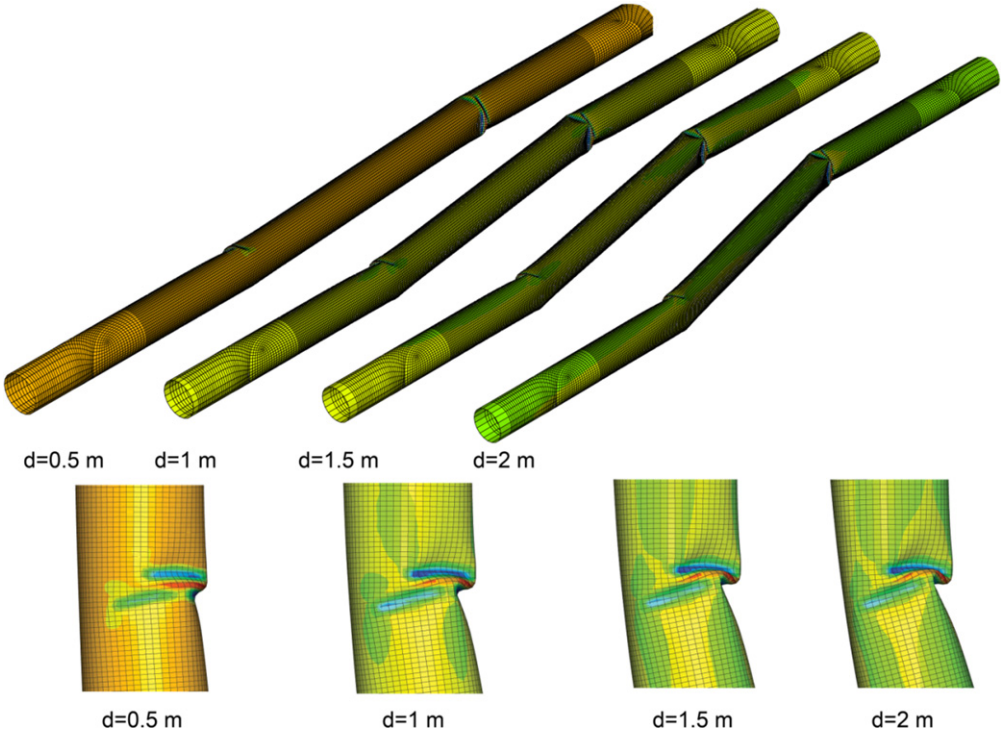

Fig. 11. (a) Deformed shapes and distribution of longitudinal strain for an X65 $D/t=96$ pipeline in Clay I conditions and $\beta=-10^{\circ}$, for various values of fault displacement and (b) corresponding cross-sectional deformation at 0.5 m from the fault.

The above numerical results for the X65-steel pipe are shown in graphical form in Fig. 12, where the fault displacement values corresponding to the performance criteria: (a) local buckling, (b) longitudinal strain equal to 3%, (c) longitudinal strain equal to 5% and (d) cross-sectional flattening $f=0.15$, are plotted with respect to the crossing angle β. The results indicate that for non-positive values of angle β, local buckling is the dominant limit state. For positive values of β, two major limit states, namely the 3% longitudinal tensile strain and the cross section flattening are most important. For values of β up to about 15 degrees, cross sectional flattening is reached first, whereas for greater values of β the 3% tensile strain criterion becomes the dominant limit state. It is further observed that an increase of the value of β results in a significant decrease of the value of critical fault displacement.

In Figs. 13–15 the fault displacement values corresponding to the three performance criteria are plotted with respect to the crossing angle β for X65 pipelines with D/t ratios equal to 144, 72 and 57.6 respectively. The results indicate that the behavior has

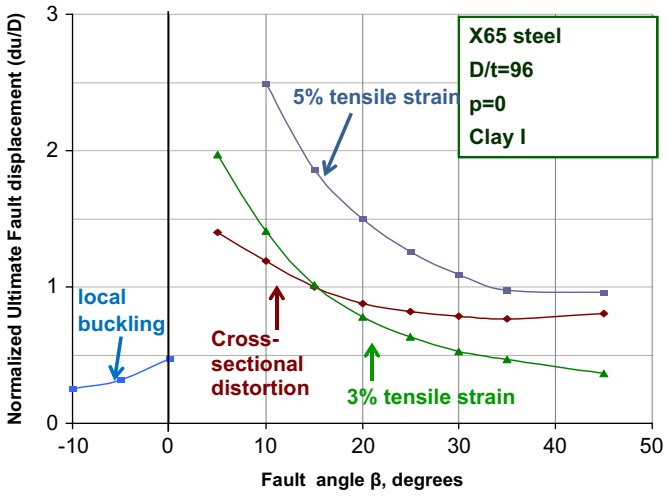

Fig. 12. Normalized ultimate fault displacement for various performance limits at different angles of β (X65 pipe, Clay I, $D/t=96$, zero pressure).

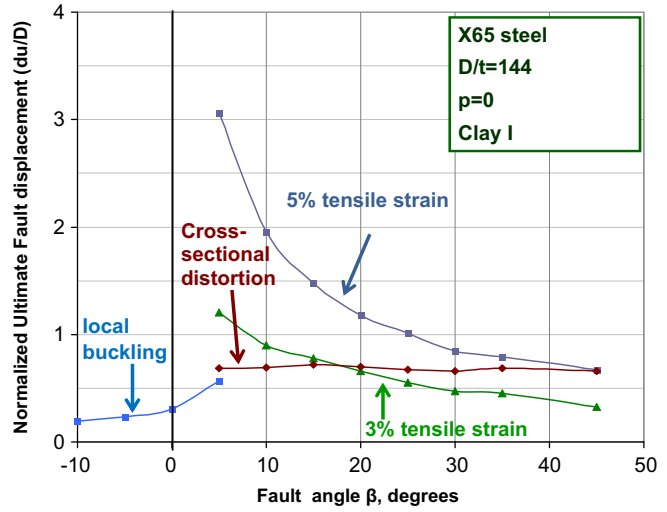

Fig. 13. Normalized ultimate fault displacement for various performance limits at different angles of β (X65 pipe, Clay I, $D/t=144$, zero pressure).

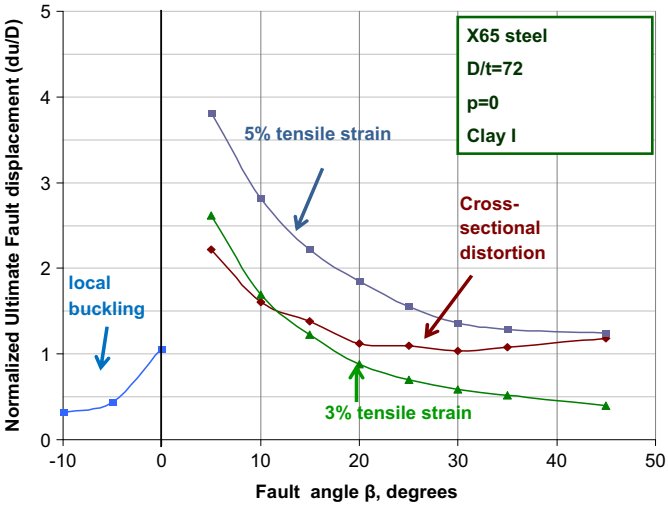

Fig. 14. Normalized ultimate fault displacement for various performance limits at different angles of β (X65 pipe, Clay I, $D/t=72$, zero pressure).

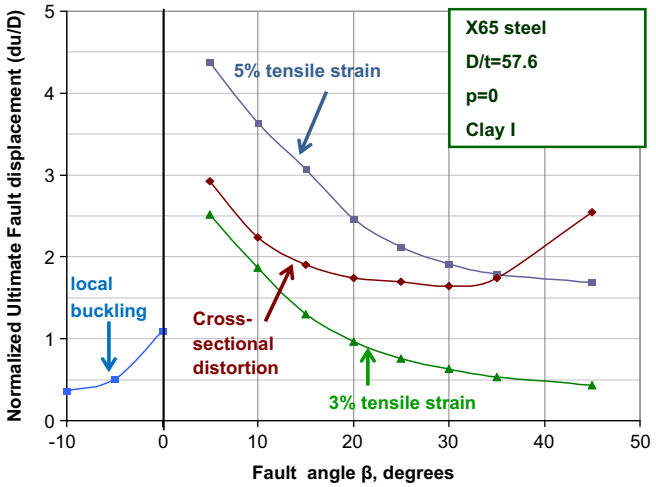

Fig. 15. Normalized ultimate fault displacement for various performance limits at different angles of β (X65 pipe, Clay I, $D/t=57.6$, zero pressure).

several similarities with the results in Fig. 12. Nevertheless, the results show a significant dependence of the critical fault displacement with respect to the D/t ratio. Local buckling is observed at non-positive values of β. In addition, for the thin-walled pipeline ($D/t=144$) local buckling may also occur for small positive values of β ($\beta=5^\circ$) at a value of fault displacement equal to 0.52 m. With increasing fault displacement, the local buckle does not develop further, and its size is reduced due to longitudinal stretching. For all cases with positive values of β, the flattening limit state and the 3% tensile strain limit state are dominant, similar to the case of $D/t=96$. The angle β at which the 3% tensile strain limit state becomes critical over the flattening limit state depends on the D/t ratio.

The response of the above X65 steel pipeline ($D/t=96$), buried in stiffer cohesive soil conditions, is examined, assuming values of soil parameters c, E and φ are equal to 200 kPa, 100 MPa and 0°, respectively. They correspond to a stiff clay under "undrained conditions", referred to as Clay II. The numerical results indicate that the bending deformation of the pipeline in stiff soil occurs within a short distance from the fault location. For the particular case of $\beta=0$, the critical cross-section is at a distance of 2.5 m from the fault. Comparison of results in Fig. 16 and with those shown in Fig. 12 (for Clay I) demonstrates the significant effect of site conditions on the response of the steel pipeline. In the case of a stiff soil, bending deformation affects a smaller length of the pipeline, so that higher bending stresses and strains develop for the same fault displacement d, than those in the case of a soft soil; thus, the performance limits for the stiff soil are reached at significantly lower value of fault displacement. Furthermore, in stiff soil conditions, Figs. 17 and 18 depict the corresponding results for X65 pipelines with D/t equal to 144 and 72. The results, compared with Figs. 12–14 indicate a significantly lower deformation capacity for those stiff soil conditions. Furthermore, the results show that for positive values of angle β the 3% tensile strain is the governing mode of failure. Depending on pipeline thickness, local buckling may also occur at positive values of angle β. More specifically, local buckling occurs for $\beta=5^\circ$ in the case of D/t equal to 72 and 96, whereas for the case of thin-walled pipeline (D/t 144) local buckling occurs even at $\beta=10^\circ$.

4.2. Non-pressurized X65 steel pipelines in cohesionless soils

The response of the above X65 steel pipeline ($D/t=96$) embedded in non-cohesive soils is examined, considering representative results for a frictional soil and comparing it to those

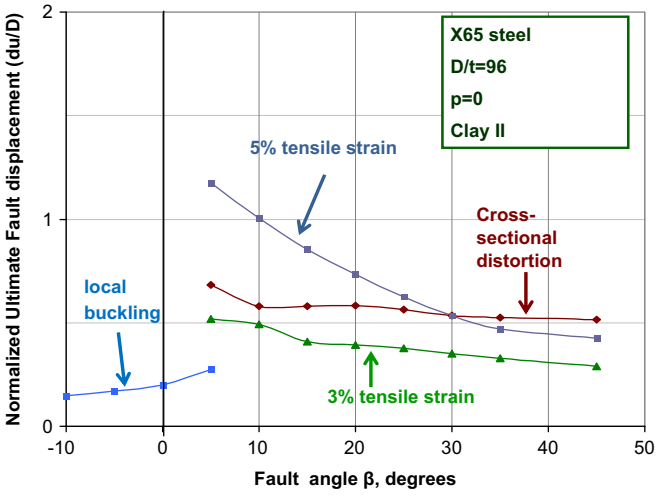

Fig. 16. Normalized ultimate fault displacement for various performance limits at different angles of β (X65 pipe, Clay II, $D/t=96$, zero pressure).

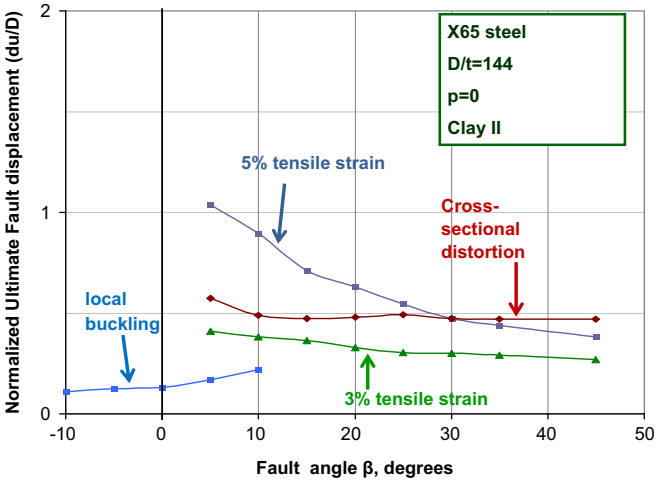

Fig. 17. Normalized ultimate fault displacement for various performance limits at different angles of β (X65 pipe, Clay II, $D/t=144$, zero pressure).

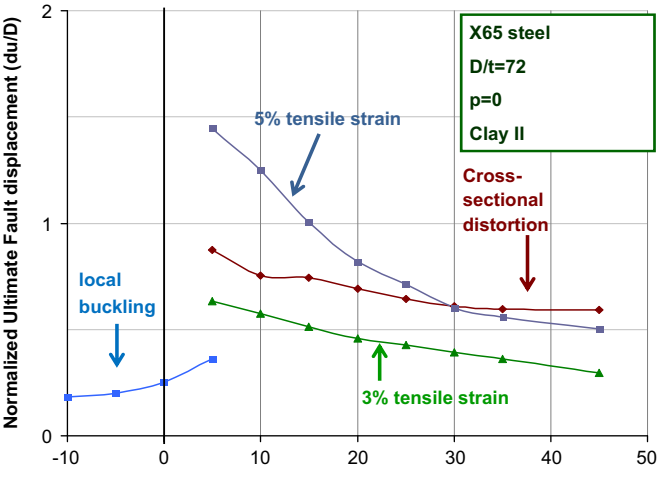

Fig. 18. Normalized ultimate fault displacement for various performance limits at different angles of β (X65 pipe, Clay II, $D/t=72$, zero pressure).

obtained for the cohesive soils. A granular soil is considered with a friction angle $\varphi=30^{\circ}$, Young's modulus $E=10$ MPa and Poisson's ratio $\nu=0.3$, corresponding to loose sand, which is referred to as "Sand". The relatively small value of the stress-depended Young's modulus E is justified by the shallow embedment depth of the pipeline. A small amount of artificial cohesion equal to $c=5$ kPa is also assumed to prevent numerical difficulties associated with the behavior of a purely frictional material at very small confining stress, such as in the case of a gap opening at the pipe–soil interface.

For various values of β, the results for the X65 pipeline with $D/t=96$ are summarized in Fig. 19. The numerical results indicate that, for non-positive values of angle β, local buckling is the dominant limit state. For the particular case of zero crossing angle ($\beta=0$), a value of fault displacement equal to 0.587 m is required for local buckling to occur. Beyond this stage, significant distortion of the cross-section occurs due to local buckling on the pipe wall on the compression side of the bent pipeline. The shape of the developing buckling is similar to that of Clay I. The longitudinal compressive strain at the onset of local buckling (ε_{cr}) is equal to 8.4×10^{-3}, higher than the value calculated via Eq. (2). For positive values of angle β up to 20 degrees, the cross-sectional flattening limit state is dominant, whereas for larger values of β the 3% tensile strain is the governing limit state.

The corresponding results for an X65 pipeline with D/t equal to 72 are depicted in Fig. 20. The behavior of this thicker buried pipeline has similar trends, but the results indicate that larger fault displacements are required in order to satisfy the criteria.

4.3. Mechanical behavior of pressurized X65 steel pipelines

The effects of internal pressure on pipeline mechanical behavior are investigated considering internally pressurized X65 pipelines with thickness of (3/8) in., embedded in soft-to-firm soil conditions (Clay I). The numerical results presented in Figs. 21 and 22 correspond to a pressure level of 38 barr, which is equal to 56% of the maximum operating pressure p_{max} expressed by Eq. (5), whereas the results in Figs. 23 and 24 show the corresponding results for a lower pressure level equal to 26 barr, which is 38% of p_{max}. At those levels of internal pressure, cross sectional distortion of the pipeline is quite small and flattening does not reach the critical value of 0.15, even for large values of the imposed fault displacement. For non-positive values of angle β local buckling occurs. The buckled shapes of the pressurized pipelines, shown in Fig. 25, are quite different from those of the non-pressurized pipelines shown in the same figure. Nevertheless, the corresponding values of critical fault displacement d_{cr} (0.41 m and 0.39 m for 38% and 56% of p_{max}) are somewhat lower

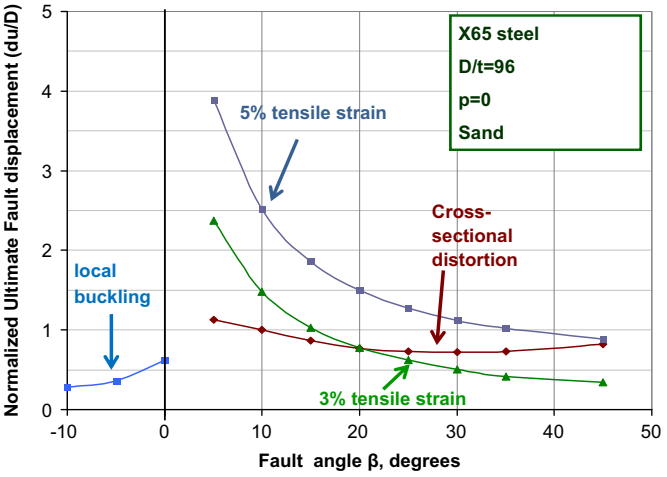

Fig. 19. Normalized ultimate fault displacement for various performance limits at different angles of β (X65 pipe, Sand, $D/t=96$, zero pressure).

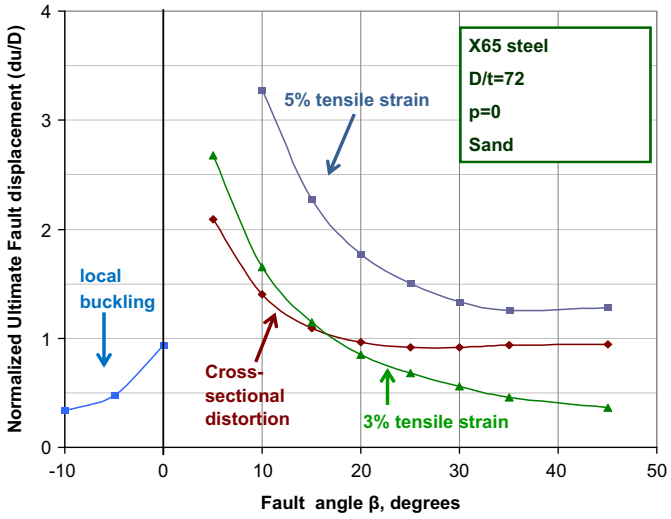

Fig. 20. Normalized ultimate fault displacement for various performance limits at different angles of β (X65 pipe, Sand, $D/t=72$, zero pressure).

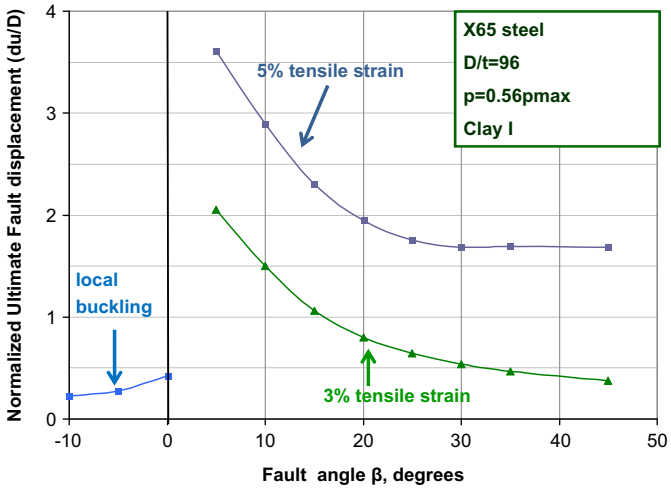

Fig. 21. Normalized ultimate fault displacement for various performance limits at different angles of β (X65 pipe, Clay I, $D/t=96$, pressure 56% of p_{max}).

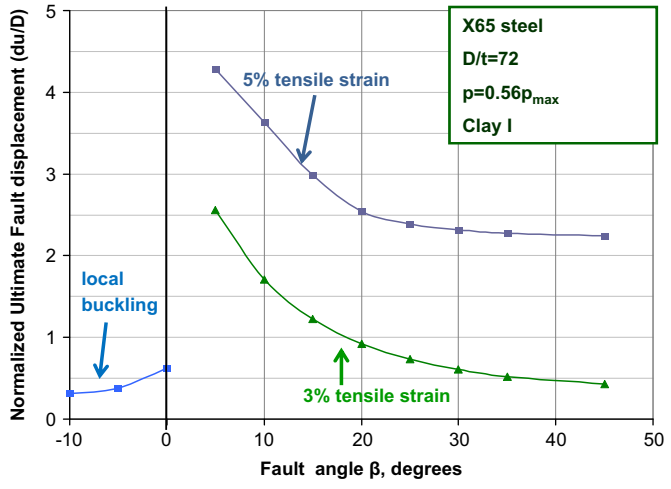

Fig. 22. Normalized ultimate fault displacement for various performance limits at different angles of β (X65 pipe, Clay I, $D/t=72$, pressure 56% of p_{max}).

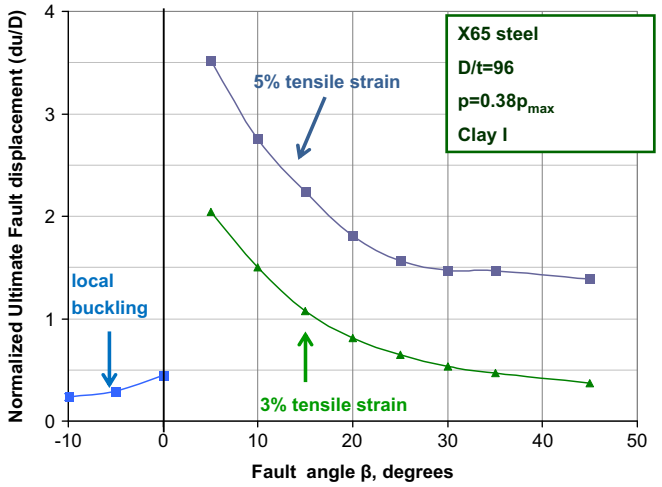

Fig. 23. Normalized ultimate fault displacement for various performance limits at different angles of β (X65 pipe, Clay I, $D/t=96$, pressure 38% of p_{max}).

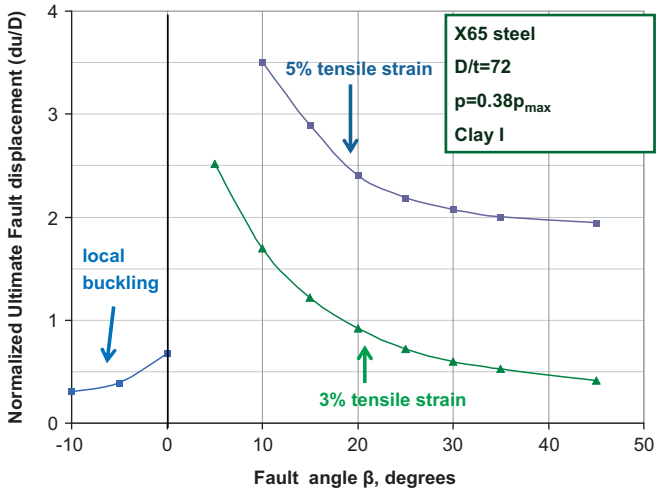

Fig. 24. Normalized ultimate fault displacement for various performance limits at different angles of β (X65 pipe, Clay I, $D/t=72$, pressure 38% of p_{max}).

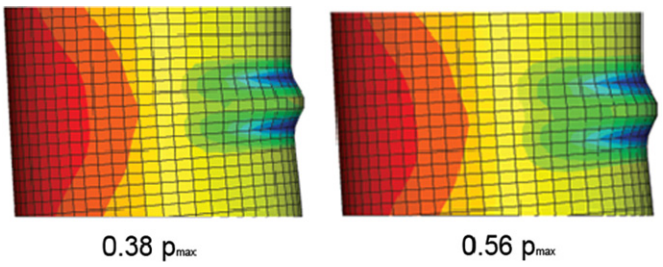

Fig. 25. Buckled shapes of pressurized pipes.

than the corresponding value without pressure. This is attributed to the development of additional stresses and strains in the pipeline wall that cause early yielding and premature local buckling formation, an observation also noted in [25]. The compressive longitudinal strains along the critical generator of the pressurized steel pipeline at the onset of local buckling are equal to -8.5×10^{-3} and -7.2×10^{-3} for 56% and 38% of p_{max}, which are higher compared to the values given from Eq. (2), equal to -4.9×10^{-3} and -3.77×10^{-3}, respectively. For positive values of angle β, the 3% longitudinal tensile strain criterion is the governing limit state.

The evolution of cross-sectional deformation in pressurized pipelines is shown in Fig. 26, in terms of flattening at the critical cross-section with respect to the applied fault displacement, for various levels of internal pressure. It is interesting to note that for rather low levels of internal pressure, the distortion of the cross-section is significantly reduced. Furthermore, in Fig. 27, the cross-sectional shape of the pressurized pipelines is depicted for the same value of fault displacement ($d=1$ m), demonstrating the effects of internal pressure on cross-sectional deformation.

Finally, the evolution of hoop, longitudinal and von Mises stresses of the pipeline pressurized at 38% of p_{max} is shown in Figs. 28–30. The stresses are measured at the cross-section where maximum stresses occur during the application of fault movement, located 0.77 m from the fault. The measurements are obtained at location A, as defined in Fig. 1c, at both the inner and the outer surface of the pipeline wall. The starting value of hoop stress is about 125 MPa, which corresponds to a level of internal pressure equal to 38% of p_{max}. For fault displacement values less than 0.25 m, the pipeline remains elastic and, because of cross-sectional flattening, hoop stress at the inner and the outer surface have opposite variations (increase of the stress at the inner surface and decrease of the stress at the outer surface). After a fault displacement of 0.25 m ($d/D \geq 0.3$), the pipeline material is no longer elastic; the small increase of longitudinal stress and the von Mises stress is due to hardening and the hoop stresses at both the inner and outer surface tend to stabilize at the initial value of 125 MPa.

4.4. Mechanical behavior of X80 steel pipelines

The behavior of buried high-strength steel X80 pipelines under fault-induced deformation is also analyzed, using the numerical tools described in the previous sections. The uniaxial nominal tensile stress–strain relationship of the API 5L X80 material is plotted in Fig. 4 with the solid curve. The material has a yield stress of 596 MPa without a plastic plateau, corresponding to a cold expanded (UOE) line pipe. The maximum operating pressure p_{max} is given by Eq. (5), and is plotted with the solid line in Fig. 5 in terms of the D/t value.

Numerical results are obtained for 36-in.-diameter X80steel pipelines with thickness equal to (3/8)-in. and (1/2)-in., corresponding to D/t values equal to 96 and 72 respectively, embedded in soft-to-firm cohesive soils (Clay I). The numerical results for zero pressure are summarized in Figs. 31 and 32, and indicate similar trends with those observed and discussed in the above

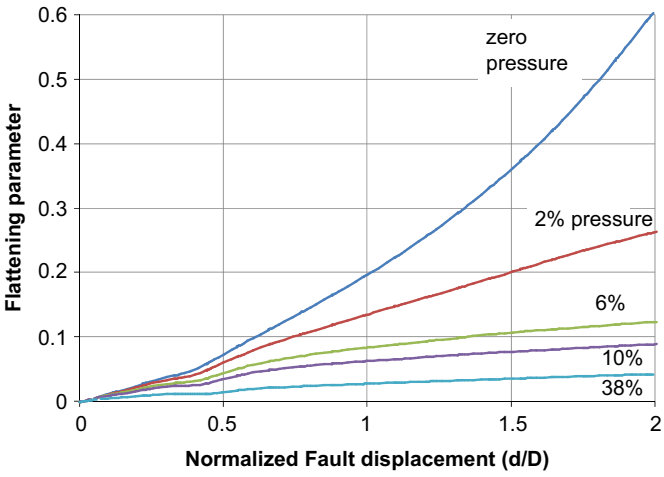

Fig. 26. Evolution of flattening parameter f versus fault displacement for different values of pressure (Clay I, X65 pipeline, $D/t=96$, $\beta=25^{\circ}$).

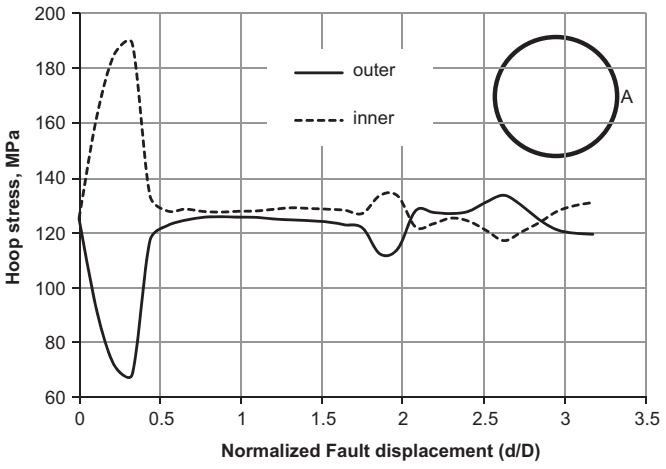

Fig. 28. Hoop stress versus fault displacement at inner and outer surface cross-section, location A, at 0.5 m from the fault (Clay I, X65 pipeline, $D/t=96$, pressure 38% of p_{max}, $\beta=25^{\circ}$).

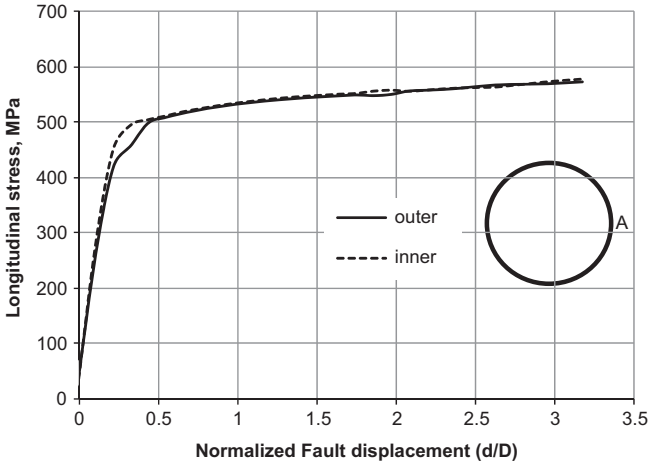

Fig. 29. Longitudinal stress versus fault displacement at inner and outer surface cross-section, location A, at 0.5 m from the fault (Clay I, X65 pipeline, $D/t=96$, pressure 38% of p_{max}, $\beta=25^{\circ}$).

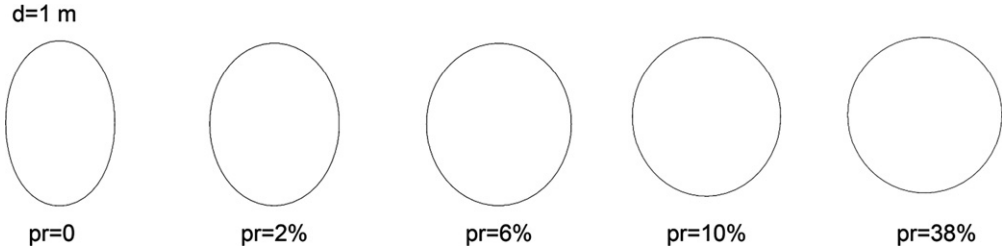

Fig. 27. Evolution of cross-sectional deformation in pressurized pipelines for the same fault displacement $d=1$ m (Clay I, X65 pipeline, $D/t=96$, $\beta=25^{\circ}$).

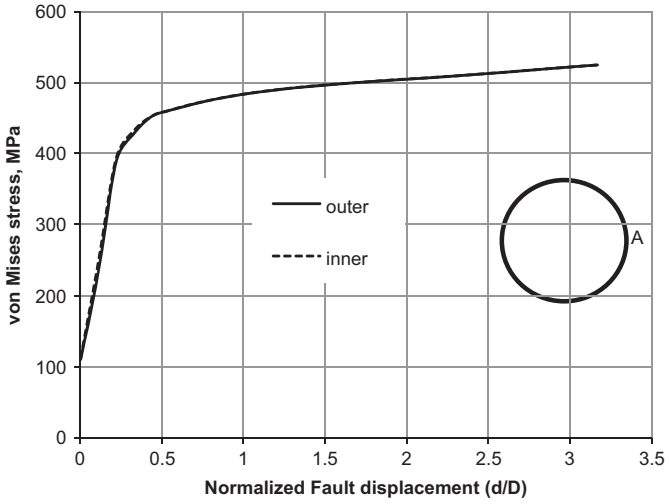

Fig. 30. Mises stress versus fault displacement at inner and outer surface cross-section, location A, at 0.5 m from the fault (Clay I, X65 pipeline, $D/t=96$, pressure 38% of p_{max}, $\beta=25^{\circ}$).

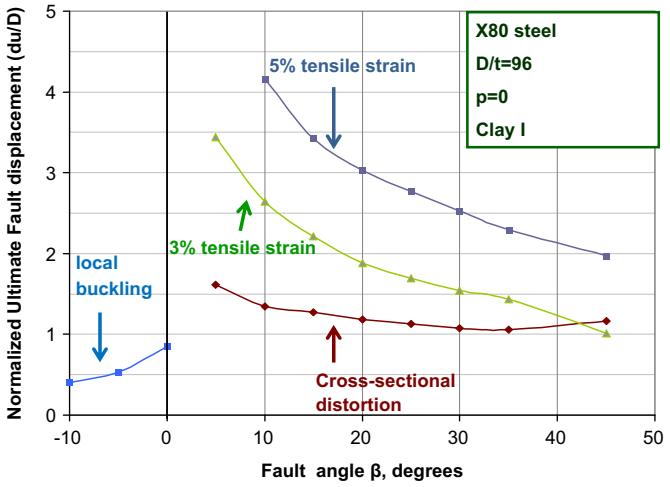

Fig. 31. Normalized ultimate fault displacement for various performance limits at different angles of β (X80 pipe, Clay I, $D/t=96$, zero pressure).

paragraphs for the X65 pipelines. In both cases, local buckling of pipeline wall occurs at non-positive values of β. A comparison of these results with those in Figs. 12 and 13 for the X65 pipelines, indicate that buckling occurs at higher values of fault displacements. Nevertheless, for the specific case where $\beta=0$ and $D/t=72$, local buckling does not occur; in this case the compressive buckling strain is rather high due to the high grade of steel and because of the tensile strains induced by longitudinal stretching, this critical strain is not reached. More details on this behavior regarding the onset of buckling are offered in Section 5, where a simplified model is presented. For positive values of angle β, the ovalization performance criterion is reached first, for both value of D/t, up to an angle of β equal to about 40 degrees.

The behavior of the pressurized X80 steel pipelines is shown in Figs. 33 and 34. For non-positive values of β, local buckling occurs and the corresponding values of critical fault displacement are similar, yet somewhat lower, than those of the non-pressurized X80 pipelines with the same D/t ratio. In addition, for positive values of angle β, cross-sectional shape of the pipeline remains quasi-circular, the flattening criterion is never reached, and the 3% longitudinal tensile strain is the governing limit state.

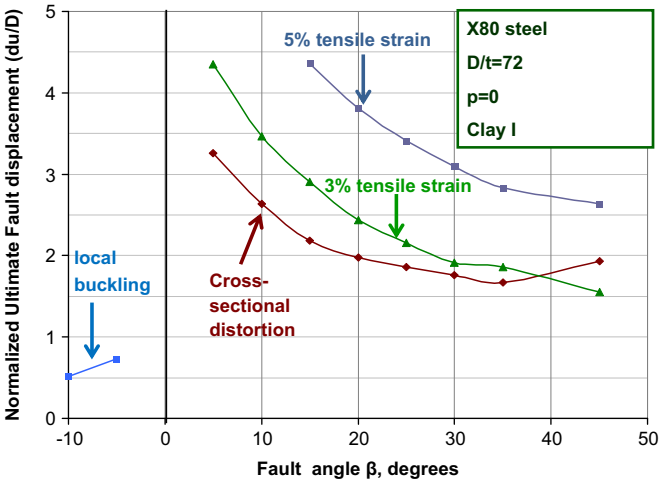

Fig. 32. Normalized ultimate fault displacement for various performance limits at different angles of β (X80 pipe, Clay I, $D/t=72$, zero pressure).

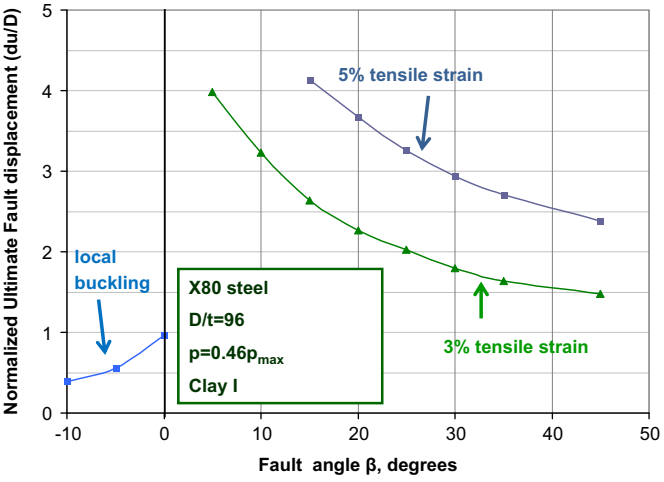

Fig. 33. Normalized ultimate fault displacement for various performance limits at different angles of β (X80 pipe, Clay I, $D/t=96$, pressure 46% of p_{max}).

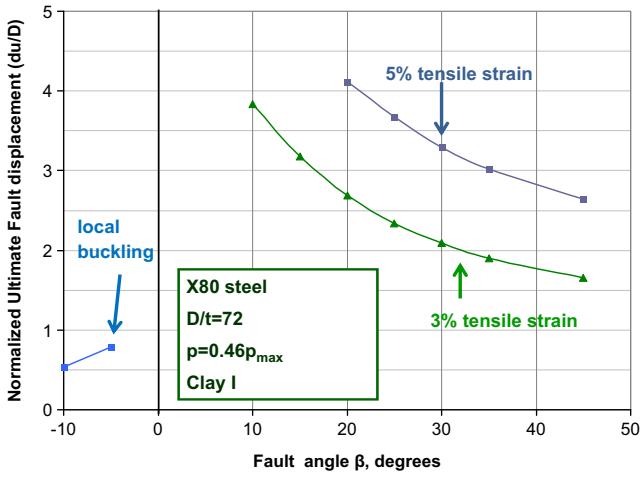

Fig. 34. Normalized ultimate fault displacement for various performance limits at different angles of β (X80 pipe, Clay I, $D/t=72$, pressure 46% of p_{max}).

5. Simplified formulation for local buckling of pipeline wall

The results obtained in the previous section indicate that for non-positive or small positive values of the crossing angle β local

buckling of pipeline wall is the governing mode of failure. Furthermore, it is shown that the occurrence of local buckling depends on several parameters related to the pipe steel grade, the soil conditions, the value of the crossing angle and the end effects. A simplified formulation is developed for describing pipeline deformation under strike-slip fault action, in order to estimate under which conditions the compressive strains that may develop in the pipeline wall could cause local buckling, considering longitudinal stretching. The present model is an improvement of the model presented in [25] for the specific case of normal fault perpendicular to the pipeline axis ($\beta=0$).

The pipeline is assumed to deform in an S-shaped "shearing type" configuration, within a segment of length L, as shown in Fig. 35. This is different than the total length of the pipeline segment L_T under consideration. It is also assumed that the pipeline shape is smooth, with circular cross-section and free of discontinuities due to local cross-sectional distortions. It is noted that buckling occurs at relative low values of fault displacement associated with rather small cross-sectional distortions. A shape function for the transverse displacement $u(x)$ of the pipeline in terms of the fault-imposed displacement d is considered in the following form:

$$u(x)=\frac{d}{2}\cos\beta\left(1-\cos\frac{\pi x}{L}\right) \tag{6}$$

where x is considered between the values of 0 and L. In addition, the axial displacement $v(x)$ of the pipeline within this segment due to stretching is assumed to be linearly distributed:

$$v(x)=\frac{d\sin\beta}{L}x \tag{7}$$

In Eq. (7), without loss of generality, it is assumed that the cross-section at $x=0$ has no axial displacement. The length L of the S-shaped deformed pipeline segment depends mainly on soil stiffness and, secondarily, by the D/t ratio.

From Eq. (6), the maximum bending curvature k, due to the imposed deformation d, can be readily computed as follows:

$$k=-\left(\frac{d^2u}{dx^2}\right)_{\max}=\frac{d\cos\beta}{2}\left(\frac{\pi}{L}\right)^2 \tag{8}$$

and assuming a circular cross-section, the corresponding bending strain ε_b

$$\varepsilon_b=\frac{kD}{2}=\frac{\pi^2}{4}\left(\frac{d\cos\beta}{L}\right)\left(\frac{D}{L}\right) \tag{9}$$

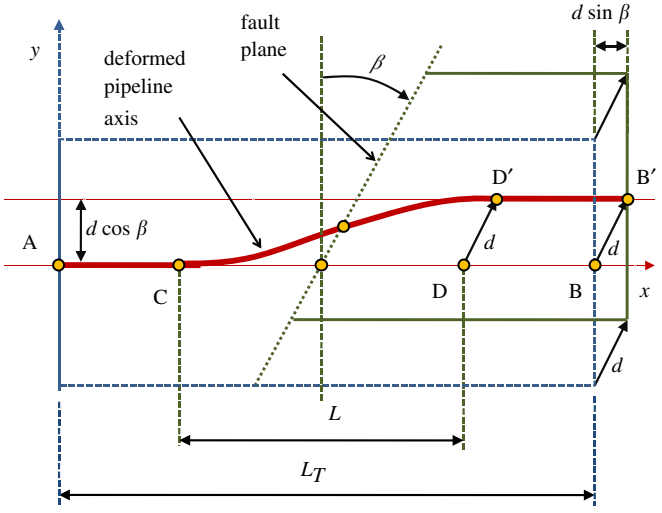

Fig. 35. Schematic representation of fault-induced deformation of pipeline axis, for the development of the simplified formulation for local buckling.

It is interesting to note that the bending strain ε_b is linear with respect to the fault displacement d.

The increase of pipeline length between cross-sections at $x=0$ and L due to pipeline stretching should also be considered. This increase of length consists mainly of two parts; the first part is due to the bending shape and the second part refers to the oblique direction of the fault with respect to the pipeline, expressed by the first two terms on the right-hand side of Eq. (10) and by the third term respectively:

$$\Delta_0=\int_0^L\sqrt{1+u'^2}dx-L+d\sin\beta \tag{10}$$

In Eq. (10), the value of Δ_0 expresses the increase of pipe length between $x=0$ and L, but neglects the axial flexibility of the pipe at the two ends of this pipeline segment, caused by pipeline continuity at these two points. Because of this axial flexibility at $x=0$ and L, the total elongation Δ of the pipeline is smaller, so that

$$\Delta=\Delta_0-\delta \tag{11}$$

where δ is a decrease of the pipe elongation due to end flexibility. Consideration of compatibility and equilibrium at $x=0$ and L, and assuming the same axial stiffness per unit length along the entire pipeline, one readily results in the following expression that relates Δ_0 and δ:

$$\frac{\Delta_0-\delta}{L}=\frac{\delta}{L_1} \tag{12}$$

or equivalently,

$$\frac{\Delta_0}{L+L_1}=\frac{\delta}{L_1} \tag{13}$$

where $L_1=L_T-L$ is the length of the pipeline outside the S-shaped pipeline segment under consideration (see also Fig. 35).

The corresponding longitudinal strain (also referred to as "membrane" strain or "stretching" strain) ε_m can be computed from Eqs. (10) and (11) as follows:

$$\varepsilon_m=\frac{\Delta}{L}=\frac{1}{L}\left(\int_0^L\sqrt{1+u'^2}dx\right)-1+\frac{d\sin\beta}{L}-\frac{\delta}{L} \tag{14}$$

which is assumed to be uniformly distributed along the pipeline segment. Using the following series expansion,

$$\sqrt{1+u'^2}=1+\frac{1}{2}u'^2+\cdots \tag{15}$$

and keeping only the first two terms, the longitudinal membrane strain from Eq. (14) becomes

$$\varepsilon_m=\frac{\Delta}{L}=\frac{1}{2L}\int_0^L u'^2dx+\frac{d\sin\beta}{L}-\frac{\delta}{L} \tag{16}$$

and considering Eqs. (10) and (13) one obtains

$$\varepsilon_m=\left(\frac{d}{L}\right)^2\frac{\pi^2\cos^2\beta}{16}\left(\frac{L}{L_T}\right)+\frac{d\sin\beta}{L}\left(\frac{L}{L_T}\right) \tag{17}$$

The longitudinal membrane strain ε_m has a linear term with respect to the fault displacement d due to the nonzero value of the crossing angle β, and a quadratic term due to pipeline bending deformation and stretching.

To compute the compressive strain ε_C, the longitudinal (tensile) membrane strain ε_m should be subtracted from the compressive bending strain ε_b. Combining Eqs. (9) and (17) one obtains the compressive strain at the critical location

$$\varepsilon_C=\varepsilon_b-\varepsilon_m \tag{18}$$

or

$$\varepsilon_C=\frac{\pi^2}{4}\left(\frac{d\cos\beta}{L}\right)\left(\frac{D}{L}\right)-\left(\frac{d}{L}\right)^2\frac{\pi^2\cos^2\beta}{16}\left(\frac{L}{L_T}\right)-\frac{d\sin\beta}{L}\left(\frac{L}{L_T}\right) \tag{19}$$

At the first stages of deformation, i.e. for small values of d, and for small values of the crossing angle β, the membrane strain ε_m is small and the bending strain ε_b governs the response. On the other hand, the membrane strain ε_m becomes dominant at later deformation stages (large values of d). The value of fault displacement at which the compressive strain ε_C reaches a maximum value is readily obtained by differentiating Eq. (18) with respect to the fault displacement d:

$$\frac{d\varepsilon_C}{dd} = \frac{\pi^2 D}{4L^2}\cos\beta - d\frac{\pi^2\cos^2\beta}{8L^2} - \frac{\sin\beta}{L} + \frac{\delta'}{L} \tag{20}$$

where δ' is the derivative of δ with respect to d. Setting the derivative, $d\varepsilon_C/dd$ equal to zero, and considering Eq. (13) for the value of δ, one obtains

$$d \equiv d_0 = \frac{2L}{\cos\beta}\left[\left(\frac{D}{L}\right)\left(\frac{L_T}{L}\right) - \frac{4\tan\beta}{\pi^2}\right] \tag{21}$$

The above expression is valid for positive values of d. This implies that

$$\left(\frac{D}{L}\right)\left(\frac{L_T}{L}\right) \geq 0.4\tan\beta \tag{22}$$

The corresponding maximum value of compressive strain ε_C is

$$\varepsilon_{C,\max} = \frac{\pi^2}{4}\left(\frac{L}{L_T}\right)\left[\left(\frac{D}{L}\right)\left(\frac{L_T}{L}\right) - \frac{4}{\pi^2}\tan\beta\right]^2 \tag{23}$$

Beyond that stage, the value of compressive strain ε_C decreases with increasing fault displacement d.

If the maximum axial compressive strain $\varepsilon_{C,\max}$ in Eq. (23) is lower than the buckling (critical) strain ε_{cr} of the pipeline wall, then local buckling of the pipeline wall may not occur. This is expressed mathematically as follows:

$$\varepsilon_{C,\max} \leq \varepsilon_{cr} \tag{24}$$

In Eq. (24), the buckling (critical) strain ε_{cr} can be written in the following simplified form [40]:

$$\varepsilon_{cr} = \alpha\left(\frac{t}{D}\right) \tag{25}$$

where α is a constant that depends primarily on the soil confinement, the presence of internal pressure and on the amplitude and shape of initial imperfections, and secondarily, on the pipeline material grade. Typical values of α range between 0.4 and 0.5 [40]. Inserting Eqs. (23) and (25) into inequality (24), one obtains the following "no buckling" condition in terms of the diameter-to-thickness ratio D/t, the dimensionless parameter α and the length-over-diameter ratio L/D of the S-shaped deformed pipeline:

$$\frac{D}{t} \leq \left(\frac{D}{t}\right)_{\lim} = 0.4\alpha\left(\frac{L_T}{L}\right)\frac{1}{[(\frac{D}{L})(\frac{L_T}{L}) - 0.4\tan\beta]^2} \tag{26}$$

Note that for fault perpendicular to the pipeline axis ($\beta=0$), one readily obtains:

$$\frac{D}{t} \leq \left(\frac{D}{t}\right)_{\lim} = 0.4\alpha\left(\frac{L}{L_T}\right)\left(\frac{L}{D}\right)^2 \tag{27}$$

Furthermore, for $L=L_T$ the above expression reduces to the simple equation reported in [25].

The above analysis shows that, in the case of strike-slip faults, in order to avoid local buckling of the pipeline, the diameter-to-thickness ratio D/t may not exceed a limit value $(D/t)_{\lim}$. Within the limitations and assumptions of the above simplified formulation, the $(D/t)_{\lim}$ value is expressed by the closed-form Eq. (26). This shows that the limit value depends on the soil conditions (which have a direct effect on the values of the L/D ratio and the dimensionless parameter α), the total pipeline length L_T, and the pipeline material grade (which has an influence on the value of α).

Eq. (26) can be used for preliminary design purposes. It can be further employed for some useful conclusions of qualitative nature, related to the finite element results presented in the previous section. The main conclusion is that that the value of $(D/t)_{\lim}$ increases with softer soil conditions (expressed by the L/D ratio), and with decreasing total length (expressed by the L/L_T ratio). Typical values of the L/D ratio for the 36-in. X65 pipelines analyzed in the previous section are 26.5 and 21 for soil conditions Clay I and Clay II respectively. Applying Eq. (26) for $L/D=26.5$, $\alpha=0.5$ and $L_T=60$ m, the $(D/t)_{\lim}$ values of 57 and 144 are obtained for $\beta=0$, and 5°, respectively. This verifies that, under Clay I conditions and for $\beta=0$, all four X65 pipelines considered in the previous section ($57.6 \leq D/t \leq 144$) exhibit local buckling, whereas for $\beta=5°$ local buckling occurs only in the thin-walled pipeline case ($D/t=144$, Fig. 13); thicker pipelines do not exhibit local buckling (Figs. 12–15). In addition, for $L/D=21$ and $\alpha=0.5$, $(D/t)_{\lim}$ values are equal to 48 and 103, for $\beta=5°$, and 10°, respectively. This result is consistent with the results shown in Figs. 16–18 under Clay II conditions; for a crossing angle value $\beta=5°$, local buckling occurs in all cases, whereas for $\beta=10°$ only the thin-walled pipeline ($D/t=144$) exhibits local buckling.

6. Conclusions

Using advanced finite element simulation tools, the mechanical behavior of buried steel pipelines crossing active strike-slip faults was investigated. The pipeline is assumed to cross the fault plane at various angles. The main target is the investigation of the effects of the crossing angle for several soil and pipe parameters. The response under various cohesive and non-cohesive soil conditions (expressed through various values of soil cohesion, friction and stiffness parameters (c, φ, E)) on the structural response of the pipe are examined, with respect to three pipeline performance criteria, namely (a) maximum tensile strain, (b) local buckling and (c) cross-section flattening, towards the development of performance-based design methodologies for buried steel pipelines.

Numerical results are obtained for various values of D/t ratio and for X65 and X80 steel pipelines, which are representative for oil and gas applications. In the majority of the cases analyzed, it is shown that local buckling is the governing mode of failure for non-positive values of the crossing angle β. For pipelines under tension (positive values of β) local buckling is not dominant; in those pipelines, the governing modes of failure are the 3% value of longitudinal tensile strain and the cross-sectional flattening. Nevertheless, buckling may also occur for small positive values of β, if the pipeline is thin-walled and the ground conditions are stiff. A simple analytical model is developed for illustrating pipeline behavior in terms of buckling, resulting to a simple "no-buckling" condition in a closed-form expression.

The numerical results are presented in diagram form for normalized ultimate fault displacement in terms of the crossing angle, and indicate a strong dependence in terms of the pipeline diameter-to-thickness ratio D/t. It is concluded that softer ground conditions result in a larger deformation capacity of the pipeline. Furthermore, the presence of internal pressure prevents cross-sectional distortion, and induces additional stresses, so that the deformation capacity of the pressurized pipeline is somewhat reduced compared with non-pressurized pipelines. The results also demonstrate the superior behavior of high-strength X80 steel pipelines with respect to that of X65 pipelines.

References

[1] Newmark NM, Hall WJ. Pipeline design to resist large fault displacement. In: Proceedings of the U.S. national conference on earthquake engineering; 1975. p. 416–25.

[2] Kennedy RP, Chow AW, Williamson RA. Fault movement effects on buried oil pipeline. Journal of Transportation Engineering, ASCE 1977;103:617–33.

[3] Kennedy RP, Kincaid RH. Fault crossing design for buried gas oil pipelines. In: Proceedings of the ASME, PVP conference, vol. 77; 1983. p. 1–9.

[4] Wang LRL, Yeh YA. A refined seismic analysis and design of buried pipeline for fault movement. Earthquake Engineering and Structural Dynamics 1985;13:75–96.

[5] Vougioukas EA, Theodossis C, Carydis PG. Seismic analysis of buried pipelines subjected to vertical fault movement. Journal of Technical Councils, ASCE 1979;105(TCI):432–41.

[6] MaCaffrey MA, O'Rourke TD. Buried pipeline response to reverse faulting during the 1971 San Fernando Earthquake. In: Proceedings of the ASME, PVP conference, vol. 77; 1983. p. 151–9.

[7] Desmod TP, Power MS, Taylor CL, Lau RW. Behavior of large-diameter pipeline at fault crossings. ASCE, TCLEE 1995;1995(6):296–303.

[8] Wang LLR, Wang LJ. Parametric study of buried pipelines due to large fault movement. ASCE, TCLEE 1995;1995(6):152–9.

[9] Takada S, Hassani N, Fukuda K. A new proposal for simplified design of buried steel pipes crossing active faults. Earthquake Engineering and Structural Dynamics 2001;2001(30):1243–57.

[10] Lillig DB, Newbury BD, Altstadt SA. The second ISOPE strain-based design symposium—a review. In: Proceedings of the international society of offshore & polar engineering conference. Osaka, Japan; 2009.

[11] Kokavessis NK, Anagnostidis GS. Finite element modelling of buried pipelines subjected to seismic loads: soil structure interaction using contact elements. In: Proceedings of the ASME PVP conference. Vancouver, BC, Canada; 2006.

[12] Karamitros DK, Bouckovalas GD, Kouretzis GP. Stress analysis of buried steel pipelines at strike-slip fault crossings. Soil Dynamics and Earthquake Engineering 2007;27:200–11.

[13] Liu M, Wang Y-Y, Yu Z. Response of pipelines under fault crossing. In: Proceedings of the international offshore and polar engineering conference. Vancouver, BC, Canada; 2008.

[14] Shitamoto H, Hamada M, Okaguchi S, Takahashi N, Takeuchi I, Fujita S. Evaluation of compressive strain limit of X80 SAW pipes for resistance to ground movement. In: Proceedings of the 20th international offshore and polar engineering conference. Beijing, China; 2010.

[15] Arifin RB, Shafrizal WM, Wan B, Yusof M, Zhao P, Bai Y. Seismic analysis for the subsea pipeline system. In: Proceedings of the ASME 2010 29th international conference on ocean, offshore and arctic engineering, OMAE2010-20671. Shanghai, China; 2010.

[16] Odina L, Tan R. Seismic fault displacement of buried pipelines using continuum finite element methods. In: Proceedings of the ASME 2009 28th international conference on ocean, offshore and arctic engineering, OMAE2009-79739. Honolulu, Hawaii; 2009.

[17] Odina L, Conder RJ. Significance of Lüder's plateau on pipeline fault crossing assessment. In: Proceedings of the ASME 2010 29th international conference on ocean, offshore and arctic engineering, OMAE2010-20715. Shanghai, China; 2010.

[18] Gu X, Zhang H. Research on aseismatic measures of gas pipeline crossing a fault for strain-based design. In: Proceedings of the ASME 2009 pressure vessels and piping division conference, PVP2009-77987; 2009.

[19] Trifonov OV, Cherniy VP. A semi-analytical approach to a nonlinear stress–strain analysis of buried steel pipelines crossing active faults. Soil Dynamics and Earthquake Engineering 2010;30:1298–308.

[20] Trifonov OV, Cherniy VP. Elastoplastic stress–strain analysis of buried steel pipelines subjected to fault displacements with account for service loads. Soil Dynamics and Earthquake Engineering 2012;33(1):54–62.

[21] Ha D, Abdoun TH, O'Rourke MJ, Symans MD, O'Rourke TD, Palmer MC, et al. Buried high-density polyethylene pipelines subjected to normal and strike-slip faulting—a centrifuge investigation. Canadian Geotechnical Journal 2008;45:1733–42.

[22] Ha D, Abdoun TH, O'Rourke MJ, Symans MD, O'Rourke TD, Palmer MC, et al. Centrifuge modelling of earthquake effects on buried high-density polyethylene (HDPE) pipelines crossing fault zones. Journal of Geotechnical and Geoenvironmental Engineering, ASCE 2008;134(10):1501–15.

[23] Abdoun TH, Ha D, O'Rourke MJ, Symans MD, O'Rourke TD, Palmer MC, et al. Factors influencing the behavior of buried pipelines subjected to earthquake faulting. Soil Dynamics and Earthquake Engineering 2009;29:415–27.

[24] Daiyan N, Kenny S, Phillips R, Popescu R. Numerical investigation of oblique pipeline/soil interaction in sand. In: Proceedings of the 8th international pipeline conference, IPC2010-31644. Calgary, Alberta, Canada; 2010.

[25] Vazouras P, Karamanos SA, Dakoulas P. Finite element analysis of buried steel pipelines under strike-slip fault displacements. Soil Dynamics and Earthquake Engineering 2010;30(11):1361–76.

[26] Wang X, Kibey S, Tang H, Cheng W, Minnaar K, Macia ML, et al. Strain-based design—advances in prediction methods of tensile strain capacity. In: Proceedings of the 20th international offshore and polar engineering conference, ISOPE 2010. Beijing, China; 2010.

[27] Canadian Standard Association. Oil and gas pipeline systems, CSA-Z662. Mississauga, Ontario, Canada; 2007.

[28] Wang YY, Horsley D, Liu M. Strain based design of pipelines. In: Proceedings of the 16th joint technical meeting. Canberra, Australia: Australian Pipeline Association; 2007.

[29] Gresnigt AM. Plastic design of buried steel pipes in settlement areas. HERON 1986;31(4):1–113.

[30] Gresnigt AM, Karamanos SA. Local buckling strength and deformation capacity of pipes. In: Proceedings of the 19th international offshore and polar engineering conference. Osaka, Japan; 2009. p. 212–23.

[31] Nederlands Normalisatie-Instituut. Requirements for pipeline systems, NEN 3650, part-1: general, and part-2: steel pipelines; 2006.

[32] ABAQUS. Users' Manual. Simulia, Providence, RI, USA; 2011.

[33] Mohitpour M, Golshan H, Murray A. Pipeline design and construction: a practical approach. 3rd ed. New York: ASME Press; 2007.

[34] Anastasopoulos I, Callerio A, Bransby MF, Davies MC, Nahas AEl, Faccioli E, et al. Numerical analyses of fault foundation interaction. Bulletin of earthquake engineering, vol. 6. Springer; 2008 [p. 645–75].

[35] Gazetas G, Anastasopoulos I, Apostolou M. Shallow and deep foundation under fault rapture or strong seismic shaking. In: Pitilakis K, editor. Earthquake geotechnical engineering. Springer; 2007. p. 185–215.

[36] Anastasopoulos, et al. Fault rupture propagation through sand: finite element analysis and validation through centrifuge experiments. Journal of Geotechnical and Geoenvironmental Engineering, ASCE 2007;133(8):943–58.

[37] Bransby MF, Davies MC, Nahas AEl. Centrifuge modeling of normal fault-foundation interaction. Bulletin of earthquake engineering, vol. 6. Springer; 2008 [p. 585–605].

[38] American Society of Mechanical Engineers. Pipeline transportation systems for liquid hydrocarbons and other liquids, ANSI/ASME B31.4; 2006.

[39] American Society of Mechanical Engineers. Gas transmission and distribution piping systems, ANSI/ASME B31.8; 2007.

[40] Comité Européen de Normalisation. Eurocode 8, part 4: silos, tanks and pipelines, CEN EN1998-4. Brussels, Belgium; 2006.

[41] American Society of Civil Engineers. Buried flexible steel pipe; design and structural analysis. In: Whidden WR, editor. ASCE manual of practice, MOP; 2009. p. 119.

[42] Dama E, Karamanos SA, Gresnigt AM. Failure of locally buckled pipelines. Journal of Pressure Vessel Technology, ASME 2007;129(2):272–9.

[43] Das S, Cheng JJR, Murray DW, Nazemi N. Effect of monotonic and cyclic bending deformations on NPS12 wrinkled steel pipeline. Journal of Structural Engineering, ASCE 2008;134(12):1810–7.